JAMES | Journal of Advances in Modeling Earth Systems

RESEARCH ARTICLE
10.1029/2019MS001867

Key Points:
- A new process-based model incorporating microbial mechanisms was developed to quantify CH_4 emissions from natural wetlands
- The model was applied to 24 different wetlands globally to compare the simulated CH_4 emissions to observations
- The sensitivity analysis showed the significant impacts of parameters regulating DOC and acetate production, and acetoclastic methanogenesis on simulated CH_4 emissions

Supporting Information:
- Supporting Information S1

Correspondence to:
W. Yuan,
yuanwp3@mail.sysu.edu.cn

Citation:
Song, C., Luan, J., Xu, X., Ma, M., Aurela, M., Lohila, A., et al. (2020). A microbial functional group-based CH_4 model integrated into a terrestrial ecosystem model: Model structure, site-level evaluation, and sensitivity analysis. *Journal of Advances in Modeling Earth Systems*, *12*, e2019MS001867. https://doi.org/10.1029/2019MS001867

Received 16 AUG 2019
Accepted 4 MAR 2020
Accepted article online 12 MAR 2020

A Microbial Functional Group-Based CH_4 Model Integrated Into a Terrestrial Ecosystem Model: Model Structure, Site-Level Evaluation, and Sensitivity Analysis

Chaoqing Song[1,2], Junwei Luan[3], Xiaofeng Xu[4], Minna Ma[5,6], Mika Aurela[7], Annalea Lohila[7], Ivan Mammarella[8], Pavel Alekseychik[8], Eeva-Stiina Tuittila[9], Wei Gong[10], Xiuzhi Chen[5,6], Xianhong Meng[11], and Wenping Yuan[5,6]

[1]State Key Laboratory of Cryospheric Sciences, Northwest Institute of Eco-Environment and Resources, Chinese Academy of Sciences, Lanzhou, China, [2]University of Chinese Academy of Sciences, Beijing, China, [3]International Center for Bamboo and Rattan, Beijing, China, [4]Department of Biology, San Diego State University, San Diego, CA, USA, [5]Guangdong Province Key Laboratory for Climate Change and Natural Disaster Studies, School of Atmospheric Sciences, Sun Yat-sen University, Zhuhai, China, [6]Southern Laboratory of Ocean Science and Engineering, Zhuhai, China, [7]Finnish Meteorological Institute, Helsinki, Finland, [8]Institute for Atmospheric and Earth System Research/Physics, Faculty of Science, University of Helsinki, Helsinki, Finland, [9]School of Forest Sciences, University of Eastern Finland, Joensuu, Finland, [10]Institute of Land Surface System and Sustainable Development, Faculty of Geographical Science, Beijing Normal University, Beijing, China, [11]Key Laboratory of Land Surface Process and Climate Change in Cold and Arid Regions, Northwest Institute of Eco-Environment and Resources, Chinese Academy of Sciences, Lanzhou, China

Abstract Wetlands are one of the most important terrestrial ecosystems for land-atmosphere CH_4 exchange. A new process-based, biophysical model to quantify CH_4 emissions from natural wetlands was developed and integrated into a terrestrial ecosystem model (Integrated Biosphere Simulator). The new model represents a multisubstance system (CH_4, O_2, CO_2, and H_2) and describes CH_4 production, oxidation, and three transport processes (diffusion, plant-mediated transport, and ebullition). The new model uses several critical microbial mechanisms to represent the interaction of anaerobic fermenters and homoacetogens, hydrogenotrophic, and acetoclastic methanogens, and methanotrophs in CH_4 production and oxidation. We applied the model to 24 different wetlands globally to compare the simulated CH_4 emissions to observations and conducted a sensitivity analysis. The results indicated that (1) for most sites, the model was able to capture the magnitude and variation of observed CH_4 emissions under varying environmental conditions; (2) the parameters that regulate dissolved organic carbon and acetate production, and acetoclastic methanogenesis had the significant impact on simulated CH_4 emissions; (3) the representation of the process components of CH_4 cycling showed that CH_4 oxidation was about half or more of CH_4 production, and plant-mediated transport was the dominant pathway at most sites; and (4) the seasonality of simulated CH_4 emissions can be controlled by soil temperature, water table position, or combinations thereof.

Plain Language Summary CH_4 emission from wetlands is an important part of global carbon cycle. A new process-based model was developed to quantify the CH_4 emission from wetlands. The new model considered main microbial mechanisms and transport processes in wetland CH_4 cycling, and the modeled results matched the observed CH_4 emissions well at evaluation sites globally. A sensitivity analysis indicated the important role of parameters that controlled dissolved organic carbon and acetate production and acetoclastic methanogenesis. The assessment of process components of CH_4 cycling demonstrated the importance of CH_4 oxidation and plant-mediated transport in wetland CH_4 emission.

1. Introduction

CH_4 is well known to be an important greenhouse gas that has about 28 times the global warming potential of CO_2 over a 100-year scale (Myhre et al., 2013). The concentration of atmospheric CH_4 has increased from 722 ± 25 ppb in 1750 to 1,803 ± 2 ppb in 2011, about 2.5 times, since preindustrial periods (Hartmann et al., 2013). Natural wetlands, including wet soils, swamps, fens, bogs, and peatlands, are the largest

individual natural CH_4 emissions source (Bridgham et al., 2013; Saunois et al., 2016). The estimation of CH_4 emissions from natural wetlands ranges from 153 to 227 Tg CH_4 per year for the 2003–2012 period, which accounts for 30% (top-down inversions) and 25% (bottom-up estimation) on the average of total CH_4 emissions (Saunois et al., 2016), meaning natural wetlands play an important role in the global CH_4 budget and climate change.

CH_4 emission from natural wetlands is a net balance between microbial CH_4 production and consumption. There exists two major CH_4 production mechanisms, hydrogenotrophic methanogenesis and acetoclastic methanogenesis (Conrad, 1999; Krüger et al., 2001); two CH_4 oxidation mechanisms, aerobic and anaerobic methanotrophy (Gerard & Chanton, 1993; Smemo & Yavitt, 2011); and three aggregated CH_4 transport pathways, plant-mediated transport, diffusion, and ebullition (Chanton, 2005; Mer & Roger, 2001; Whiting & Chanton, 1996), all of which are influenced by the availability and quality of substrate, soil temperature and pH, hydrological conditions, and vegetation composition, and so forth (Walter & Heimann, 2000). In anaerobic conditions, organic polymers are utilized by fermenters plus H_2-producing acetogens to generate acetate, CO_2, and H_2, which become the substrates for hydrogenotrophic methanogens and acetoclastic methanogens and are ultimately transformed into CH_4. After CH_4 is produced, it can be oxidized by methanotrophs to form CO_2 or be transported via vascular plants, molecular diffusion, and bubbles (Riley et al., 2011).

Numerous process-based models have been developed to quantify CH_4 emissions from natural wetlands during the past decades, including WMEM (Cao et al., 1996), the Arah model (Arah & Stephen, 1998), ecosys (Grant, 1998, 1999), the Walter model (Walter & Heimann, 2000), Wetland-DNDC (Zhang et al., 2002), the Kettunen model (Kettunen, 2003), PEATLAND-VU (Van Huissteden et al., 2006), TEM-CH_4 (Tang et al., 2010; Zhuang et al., 2004), DLEM (Tian et al., 2010), ORCHIDEE (Ringeval et al., 2010, 2011), LPJ-WHyMe (Wania et al., 2010), CLM4Me (Riley et al., 2011), VISIT (Ito & Inatomi, 2012), TRIPLEX-GHG (Zhu et al., 2014), CLM-Microbe (Xu et al., 2015), JSBACH-methane (Kaiser et al., 2017), TECO_SPRUCE_ME (Ma et al., 2017), HIMMELI (Raivonen et al., 2017), and the soil methane scheme of ISBA (Morel et al., 2019). These models explicitly consider CH_4-related biogeochemical processes and their responses to environmental factors, and many of them simultaneously account for CH_4 production, oxidation, and three transport pathways. On the whole, these models share the following features: (1) the majority of models use a simple function directly associated with soil heterotrophic respiration, dissolved organic carbon (DOC), or environmental factors to estimate CH_4 production, lacking the representation of key microbial mechanisms; (2) the diffusion and ebullition processes are usually simulated as a threshold phenomenon whereby gas is released once the gas concentration exceeds a prescribed threshold concentration; and (3) many models have only been evaluated with a few in situ observations, without being compared against continuous CH_4 measurements collected over large spatial scales (only Riley et al., 2011 and Zhu et al., 2014 compared simulated and observed CH_4 emissions across different wetlands globally).

Using existing observations and studies, these models predict wetland CH_4 fluxes at ecosystem, regional and global scales. Yet recent studies have indicated that most previous models reproduced regional- to global-scale observations poorly (Bohn et al., 2015; Bohn & Lettenmaier, 2010). A recent model intercomparison project showed that the maximum estimate of global wetland CH_4 emissions is 264 Tg CH_4 per year, which is 1.89 times the minimum estimate of 141 Tg CH_4 per year (Melton et al., 2013). In addition, it is important to accurately quantify the response of global wetland CH_4 emissions to climate change, but Melton et al. (2013) found that the sign and magnitude of CH_4 emissions response to changes in temperature and precipitation vary among the models. Furthermore, only a few of the above models consider the interaction of different gases during the vertical migration of CH_4; for example, the Arah model (Arah & Stephen, 1998), CLM4Me (Riley et al., 2011), and JSBACH-methane (Kaiser et al., 2017) account for CH_4 and O_2 simultaneously; LPJ-WHyMe (Wania et al., 2010), HIMMELI (Raivonen et al., 2017), and the soil methane scheme of ISBA (Morel et al., 2019) take CH_4, O_2, and CO_2 into consideration by keeping track of their dynamics throughout the process; and TEM-CH_4 (Tang et al., 2010) incorporates N_2-related processes to make it a four-substance model that can resolve CH_4 biogeochemical cycling. Meanwhile, only three models incorporate the critical microbial mechanisms for CH_4 production and oxidation, including hydrogenotrophic methanogenesis, acetoclastic methanogenesis, and methanotrophy (e.g., Grant, 1998, 1999; Kettunen, 2003; Xu et al., 2015).

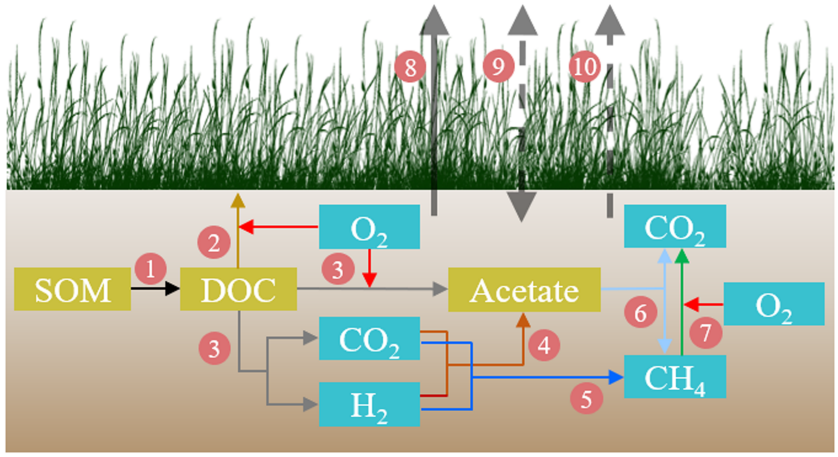

Figure 1. Schematic representation of key processes in the new wetland CH_4 model. The numbers in the red circle patterns are (1) soil organic matter decomposition, (2) aerobic respiration, (3) DOC decomposition (including fermentation and aerobic decomposition), (4) homoacetogenesis, (5) hydrogenotrophic methanogenesis, (6) acetoclastic methanogenesis, (7) CH_4 oxidation, (8) diffusion, (9) plant-mediated transport, and (10) ebullition. The red arrows represent the processes involving O_2, including aerobic respiration, aerobic decomposition of DOC, and CH_4 oxidation.

In this study, we developed a new process-based model to quantify CH_4 emissions from natural wetlands, which considered the interaction of different gases, including CH_4, O_2, CO_2, and H_2, and incorporated the main microbial mechanisms related to CH_4 production and oxidation. Moreover, the new process-based model has been integrated in a terrestrial ecosystem model (Integrated Biosphere Simulator [IBIS]), which can reflect interactions between soil temperature, hydrology, vegetation, and CH_4 biogeochemical processes. The aims of this study are to (a) introduce a new wetland CH_4 emission model that includes the explicit description of the microbial mechanisms related to CH_4 generation, (b) show the capability of this model to simulate CH_4 emissions from natural wetlands by comparing with 24 site-level observations globally, and (c) assess the process components of wetland CH_4 cycling and the control on the seasonality of modeled CH_4 emissions.

2. Model Description

A new representation of natural wetland CH_4 emissions within a terrestrial ecosystem model, the IBIS, was developed for this study. The IBIS is a process-based, comprehensive model that describes land surface processes, terrestrial carbon balance, and vegetation dynamics. The main processes represented in the IBIS model include land surface physics, canopy physiology, phenology, vegetation structure and competition, and carbon and nitrogen cycling in the terrestrial biosphere and have been integrated into a single, physically consistent, with different time scales, modeling framework (Foley et al., 1996; Kucharik et al., 2000; Liu et al., 2014; Yuan et al., 2014); here, we only describe the development of novel wetland CH_4 dynamics. The new wetland CH_4 emission model (Figure 1) is a multidimensional substance system that simulates the biogeochemical processes related to CH_4, O_2, CO_2, and H_2 and accounts for the transient, vertically resolved dynamics of these gases. The model introduces specific microbial mechanisms like anaerobic fermentation and homoacetogenesis, hydrogenotrophic methanogenesis, acetoclastic methanogenesis, and methanotrophy to account for CH_4 production and oxidation. To calculate net CH_4 emissions, the model also explicitly considers three different transport pathways including molecular diffusion, plant-mediated transport, and ebullition.

The transient reaction-diffusion equations governing the concentrations of CH_4, O_2, CO_2, H_2, and Ace (acetate) are:

$$\frac{\partial}{\partial t}C_{CH_4}(z,t) = \frac{\partial}{\partial z}F_{diff,CH_4} - Q_{plant,CH_4} - Q_{ebull,CH_4} + R_{prod,CH_4} - R_{oxid,CH_4}, \quad (1)$$

$$\frac{\partial}{\partial t}C_{O_2}(z,t) = \frac{\partial}{\partial z}F_{diff,O_2} - Q_{plant,O_2} - Q_{ebull,O_2} - R_{aero} - 2R_{oxid,CH_4}, \quad (2)$$

$$\frac{\partial}{\partial t}C_{CO_2}(z,t) = \frac{\partial}{\partial z}F_{diff,CO_2} - Q_{plant,CO_2} - Q_{ebull,CO_2} + R_{prod,CO_2} - R_{cons,CO_2}, \tag{3}$$

$$\frac{\partial}{\partial t}C_{H_2}(z,t) = \frac{\partial}{\partial z}F_{diff,H_2} - Q_{plant,H_2} - Q_{ebull,H_2} + R_{prod,H_2} - R_{cons,H_2}, \tag{4}$$

$$\frac{\partial}{\partial t}C_{Ace}(z,t) = R_{prod,Ace} - R_{cons,Ace}, \tag{5}$$

where $C_X(z,t)$ is the concentration of compound X at soil layer depth z and time t; $F_{diff,X}$ is the diffusive flux of compound X; $Q_{plant,X}$ and $Q_{ebull,X}$ are the transport rates of compound X via plant aerenchyma and ebullition, respectively; $R_{prod,X}$ is the production rate of compound X, R_{oxid,CH_4} is the CH_4 oxidation rate; $R_{cons,X}$ is the consumption rate of compound X; and R_{aero} represents the aerobic respiration rate.

Water table depth is an important factor that separates the whole soil column into aerobic and anaerobic zones. In this study, site-level water table depth observations were used. We assume that CH_4 is produced in the layers below the water table position and mainly consumed in the layers above the water table position (Walter & Heimann, 2000). The original IBIS included six soil layers with thicknesses of 0.1, 0.15, 0.25, 0.5, 1.0, and 2.0 m, with a total soil depth of 4 m (Foley et al., 1996). In order to represent water table depth specifically, we divided the soil column into nine layers, with the first five layers having a thickness of 0.1 m and the other four layers having thicknesses of 0.2, 0.3, 0.5, and 0.5 m, respectively. We only considered the CH_4-related biogeochemical processes occurring in the nine soil layers. The detailed algorithms are described as follows.

2.1. CH_4 Production

2.1.1. Available Carbon Decomposition

Methanogens prefer fresh organic matter as their substrate (Joabsson & Christensen, 2001), so the initial carbon source available for methanogens mainly comprises easily decomposed plant litterfall and root exudates. Given that DOC is a key intermediate for anaerobic fermentation and is converted from hydrolysis products and eventually decomposed into acetate, CO_2, and H_2, we define it to be the original, available carbon for methanogens and use a simple formula for its calculation:

$$DOC = K_{cpool} \times \frac{cpool}{dz} \times f_T(DOCprodQ_{10}) \times f_{moist}. \tag{6}$$

Here, DOC is the dissolved organic carbon concentration (mol m^{-3}), K_{cpool} represents the ratio of DOC to soil organic carbon, cpool is the soil organic carbon content (mol m^{-2}), dz is the layer thickness (m), $DOCprodQ_{10}$ is the temperature sensitivity of DOC production, f_T and f_{moist} are soil temperature and moisture factors, respectively. We use the approach adopted by Wania et al. (2010) and Raivonen et al. (2017) to distribute the available carbon for methanogens to all soil layers according to the root fraction f_{root}, which is calculated in the IBIS.

Under anaerobic conditions, the available carbon is fermented into acetate, CO_2, and H_2, which is governed by the following equation:

$$DOC \rightarrow 0.67Ace + 0.33CO_2 + 0.11H_2. \tag{7}$$

Thus, the fermentation is presented as:

$$DOCprodAce = V_{DOCprodAce,max} \times \frac{DOC}{K_{DOCprodAce} + DOC} \times f_T(AceprodQ_{10}) \times f_{pH}, \tag{8}$$

$$DOCprodCO2 = 0.5 \times DOCprodAce, \tag{9}$$

$$DOCprodH2 = \frac{1}{6} \times DOCprodAce. \tag{10}$$

Under aerobic conditions, the available carbon is decomposed into acetate and CO_2, which can be calculated as

$$\mathrm{DOCprodAce} = \mathrm{V}_{\mathrm{DOCprodAce,max}} \times \frac{\mathrm{DOC}}{\mathrm{K}_{\mathrm{DOCprodAce}} + \mathrm{DOC}} \times \frac{[\mathrm{O}_2]}{\mathrm{K}_{\mathrm{AceprodO2}} + [\mathrm{O}_2]} \times f_{\mathrm{T}}(\mathrm{AceprodQ}_{10}) \times f_{\mathrm{pH}}, \tag{11}$$

$$\mathrm{DOCprodCO2} = 0.5 \times \mathrm{DOCprodAce}. \tag{12}$$

Here, DOCprodAce, DOCprodCO2, and DOCprodH2 are the production rate (mol m^{-3} d^{-1}) of acetate, CO_2, and H_2, respectively. $V_{DOCprodAce,max}$ is the maximum acetate production rate (mol m^{-3} d^{-1}), $[O_2]$ is the O_2 concentration (mol m^{-3}), and $K_{DOCprodAce}$ and $K_{AceprodO2}$ are the half saturation coefficients (mol m^{-3}) for DOC and O_2, respectively. $AceprodQ_{10}$ is the temperature sensitivity of acetate production, and f_{pH} is the soil pH factor.

2.1.2. Homoacetogenesis and Hydrogenotrophic Methanogenesis

The products CO_2 and H_2 are substrates for homoacetogens and hydrogenotrophic methanogens (Grant, 1998; Grant & Roulet, 2002). At low temperature, CO_2 and H_2 appear to be the main substrates for homoacetogens, which use CO_2 as the electron acceptor to convert H_2 to acetate (chemolithotrophic acetogenesis/homoacetogenesis) (Kotsyurbenko et al., 2001; Liu & Conrad, 2011; Schulz & Conrad, 1996). This process is governed by the following equation:

$$4\mathrm{H}_2 + 2\mathrm{CO}_2 \rightarrow \mathrm{CH}_3\mathrm{COOH} + 2\mathrm{H}_2\mathrm{O}. \tag{13}$$

Thus, acetate production from homoacetogenesis is calculated as

$$\mathrm{H2prodAce} = \mathrm{V}_{\mathrm{H2prodAce,max}} \times \mathrm{Homoacetogens} \times \frac{[\mathrm{H}_2]}{\mathrm{K}_{\mathrm{H2prodAce}} + [\mathrm{H}_2]} \times \frac{[\mathrm{CO}_2]}{\mathrm{K}_{\mathrm{CO2prodAce}} + [\mathrm{CO}_2]} \times f_{\mathrm{T1}} \times f_{\mathrm{pH}}. \tag{14}$$

Here, H2prodAce is the acetate production rate from homoacetogenesis (mol m^{-3} d^{-1}), $V_{H2prodAce,max}$ is the maximum acetate production rate (mol m^{-3} d^{-1}), Homoacetogens is the microbial biomass of homoacetogens (mol m^{-3}), $[H_2]$ and $[CO_2]$ are the concentrations of H_2 and CO_2 (mol m^{-3}), $K_{H2prodAce}$ and $K_{CO2prodAce}$ are the half saturation coefficients (mol m^{-3}) for H_2 and CO_2, respectively, and f_{T1} represents the soil temperature factor.

In contrast, at high temperature, produced CO_2 and H_2 have usually been found to be suitable substrates for hydrogenotrophic methanogens (Hattroi, 2008), which use CO_2 and H_2 to generate CH_4 (hydrogenotrophic methanogenesis). This process is governed by the following equation:

$$4\mathrm{H}_2 + \mathrm{CO}_2 \rightarrow \mathrm{CH}_4 + 2\mathrm{H}_2\mathrm{O}. \tag{15}$$

Thus, CH_4 production from hydrogenotrophic methanogenesis is calculated as

$$\mathrm{H2prodCH4} = \mathrm{V}_{\mathrm{H2prodCH4,max}} \times \mathrm{H2methanogens} \times \frac{[\mathrm{H}_2]}{\mathrm{K}_{\mathrm{H2prodCH4}} + [\mathrm{H}_2]} \times \frac{[\mathrm{CO}_2]}{\mathrm{K}_{\mathrm{CO2prodCH4}} + [\mathrm{CO}_2]} \times f_{\mathrm{T2}} \times f_{\mathrm{pH}}. \tag{16}$$

Here, H2prodCH4 is the CH_4 production rate from hydrogenotrophic methanogenesis (mol m^{-3} d^{-1}), $V_{H2prodCH4,max}$ is the maximum CH_4 production rate (mol m^{-3} d^{-1}), H2methanogens is the microbial biomass of hydrogenotrophic methanogens (mol m^{-3}), $K_{H2prodCH4}$ and $K_{CO2prodCH4}$ are the half saturation coefficients (mol m^{-3}) for H_2 and CO_2, respectively, and f_{T2} represents the soil temperature factor.

2.1.3. Acetoclastic Methanogenesis

Product acetate is the substrate for acetoclastic methanogens (Grant, 1998; Grant & Roulet, 2002). CH_4 production from acetoclastic methanogenesis is governed by the following equation:

$$\mathrm{CH}_3\mathrm{COOH} \rightarrow \mathrm{CH}_4 + \mathrm{CO}_2. \tag{17}$$

Thus, CH_4 production is calculated as

$$\mathrm{AceprodCH4} = \mathrm{K_{CH4prod}} \times \left(1 - \mathrm{Grow_{Acemethanogens}}\right) \times \mathrm{Acecons}. \tag{18}$$

The acetate consumption is calculated as

$$\mathrm{Acecons} = \mathrm{V_{Acecons,max}} \times \mathrm{Acemethanogens} \times \frac{\mathrm{Ace}}{\mathrm{K_{AceprodCH4}} + \mathrm{Ace}} \times f_{\mathrm{T}}(\mathrm{CH4prodQ_{10}}) \times f_{\mathrm{pH}}. \tag{19}$$

Here, AceprodCH4 is the CH_4 production rate from acetate consumption (mol m^{-3} d^{-1}), $K_{CH4prod}$ is the CH_4 production ratio, $Grow_{Acemethanogens}$ is the growth efficiency of acetoclastic methanogens, Acecons is the acetate consumption rate for respiration by acetoclastic methanogens (mol m^{-3} d^{-1}), $V_{Acecons,max}$ is the maximum acetate consumption rate (mol m^{-3} d^{-1}), Acemethanogens is the microbial biomass of acetoclastic methanogens (mol m^{-3}), Ace is the acetate concentration (mol m^{-3}), $K_{AceprodCH4}$ is the half saturation coefficient (mol m^{-3}) for acetate, and $CH4prodQ_{10}$ is the temperature sensitivity of CH_4 production during acetate consumption.

2.2. CH_4 Oxidation

The CH_4 produced by hydrogenotrophic methanogens and acetoclastic methanogens is the substrate for methanotrophs (Grant, 1999; Grant & Roulet, 2002). In this process, heterotrophic methanotrophs are the main microbial functional group (Riley et al., 2011). We use double Michaelis-Menten kinetics to represent CH_4 oxidation, which is governed by the following equation:

$$\mathrm{CH_4} + 2\mathrm{O_2} \rightarrow \mathrm{CO_2} + 2\mathrm{H_2O}. \tag{20}$$

Thus, the R_{oxid,CH_4} (mol m^{-3} d^{-1}) is calculated as

$$\mathrm{R_{oxid,CH_4}} = \mathrm{V_{CH4oxid,max}} \times \mathrm{Methanotrophs} \times \frac{[\mathrm{CH_4}]}{\mathrm{K_{CH4oxidCH4}} + [\mathrm{CH_4}]} \times \frac{[\mathrm{O_2}]}{\mathrm{K_{CH4oxidO2}} + [\mathrm{O_2}]} \times f_{\mathrm{T}}(\mathrm{CH4oxidQ_{10}}) \times f_{\mathrm{pH}}. \tag{21}$$

Here, $V_{CH4oxid,max}$ is the maximum CH_4 oxidation rate (mol m^{-3} d^{-1}), Methanotrophs is the microbial biomass of methanotrophs (mol m^{-3}), $[CH_4]$ is the CH_4 concentration (mol m^{-3}), $K_{CH4oxidCH4}$ and $K_{CH4oxidO2}$ are the half saturation coefficients (mol m^{-3}) for CH_4 and O_2, respectively, and $CH4oxidQ_{10}$ is the temperature sensitivity of CH_4 oxidation.

O_2 is not only used to oxidize CH_4 but also consumed by aerobic respiration. We assume that part of the available carbon will be used by aerobic microbes, and this process requires O_2, so refer to Kettunen (2003); the R_{aero} (mol m^{-3} d^{-1}) is calculated as

$$\mathrm{R_{aero}} = \mathrm{K_{aer}} \times \frac{\mathrm{DOC}}{\mathrm{K_{aerDOC}} + \mathrm{DOC}} \times \frac{[\mathrm{O_2}]}{\mathrm{K_{aerO2}} + [\mathrm{O_2}]} \times f_{\mathrm{T}}(\mathrm{DOCprodQ_{10}}) \times f_{\mathrm{pH}}. \tag{22}$$

Here, K_{aer} is the O_2 consumption rate by aerobic respiration (mol m^{-3} d^{-1}), and K_{aerDOC} and K_{aerO2} are the half saturation coefficients (mol m^{-3}) for DOC and O_2, respectively.

In the above processes, $R_{prod,X}$ (mol m^{-3} d^{-1}) is the sum of produced compound X, and $R_{cons,X}$ (mol m^{-3} d^{-1}) is the sum of consumed compound X.

2.3. CH_4 Transportation

2.3.1. Diffusion

Molecular diffusive flux $F_{diff,X}$ (mol m^{-2} d^{-1}) within the soil profile depends on the vertical concentration gradient and the diffusion coefficients of compound X. Fick's first law is applied to calculate the diffusive flux (Walter & Heimann, 2000).

$$\mathrm{F_{diff,X}} = \mathrm{D_X} \frac{\partial \mathrm{C_X}}{\partial z}. \tag{23}$$

Here, D_X is the effective diffusivity of compound X (m^2 s^{-1}). We also use the constant reduction factors $f_{D,w}$ and $f_{D,a}$ to calculate the effective diffusivities in water or air (Raivonen et al., 2017), respectively.

$$D_{X,w} = f_{D,w} \times D_X^{water}, \tag{24}$$

$$D_{X,a} = f_{D,a} \times D_X^{air}. \tag{25}$$

Here, $D_{X,w}$ and $D_{X,a}$ represent the effective diffusivities of compound X in water and air ($m^2\ s^{-1}$), and D_X^{water} and D_X^{air} are the free-water and free-air diffusivities ($m^2\ s^{-1}$), respectively.

At the air-water interface, diffusivities can vary by at least four orders of magnitude. The method adopted by Wania et al. (2010) is used to calculate gas fluxes from the top soil layer into the atmosphere.

$$F_{diff,X} = -\varphi_X \times \left(C_{surf,X} - C_{eq,X}\right). \tag{26}$$

Here, $C_{surf,X}$ is the concentration of compound X in the top soil layer (mol m^{-3}), and $C_{eq,X}$ is the equilibrium concentration of compound X in the atmosphere (mol m^{-3}). φ_X represents the transfer velocity of compound X (cm hr^{-1}). We use a normalized transfer velocity φ_{600} (Cole & Caraco, 1998) to calculate the φ_X.

$$\varphi_X = \varphi_{600} \times \left(\frac{Sc_X}{600}\right)^n. \tag{27}$$

The φ_{600} (cm hr^{-1}) is calculated as

$$\varphi_{600} = 2.07 + 0.215 \times U_{10}{}^{1.7}. \tag{28}$$

Here, Sc_X is the Schmidt number of compound X, 600 is the Schmidt number for CO_2 at 20 °C, $n = -0.5$, and U_{10} is the wind speed at 10-m height (m s^{-1}). In this study, we also assume that wind speed can be ignored within the wetland vegetation so use a constant value of 0 for U_{10}. The unit of φ_X is centimeter per hour, which can be further transformed into meter per day.

For the concentration $C_{eq,X}$, which is in equilibrium with the gas partial pressure PP_X (Pa) and can be computed as:

$$C_{eq,X} = PP_X \times H_X. \tag{29}$$

Here, H_X is the Henry's law constant for compound X (mol m^{-3} Pa^{-1}). Based on the above equations, the diffusive flux for compound X can be obtained. The solution for diffusion within the soil column is obtained using the Crank-Nicholson scheme (Press et al., 1996).

2.3.2. Plant Transport

Many wetland vascular plants develop aerenchyma in response to the inundation environment. These tissues can act as conduits for the transport of CH_4, O_2, CO_2, and H_2 between the soil and atmosphere. Thus, plant-mediated transport is a diffusion process through the aerenchyma and driven by the specific gas concentration gradient (Riley et al., 2011). We refer to the approach adopted by Stephen et al. (1998) to calculate the plant transport rate $Q_{plant,X}$ (mol m^{-3} d^{-1}).

$$Q_{plant,X} = \frac{D_{air,X}}{\tau} \times \varepsilon(z) \times \frac{C_X(z,t) - C_{eq,X}}{z}. \tag{30}$$

Here, $\varepsilon(z)$ is the density of cross-sectional area of root endings at depth z ($m^2\ m^{-3}$), and τ is the root tortuosity. The effective diffusivities in air are used as the diffusion coefficients inside roots for each gas. Similar to Raivonen et al. (2017), $\varepsilon(z)$ is formulated as

$$\varepsilon(z) = a_{mA} \times \frac{f_{root}}{dz} \times \frac{LAI}{SLA}. \tag{31}$$

Here, a_{mA} is the cross-sectional area of root endings per root biomass ($m^2\ kg^{-1}$), SLA represents the specific leaf area ($m^2\ kg^{-1}$), and LAI is the leaf area index ($m^2\ m^{-2}$), which is modeled in IBIS.

2.3.3. Ebullition

Ebullition is a relatively rapid process and only occurs in water-filled soil when the total partial pressure of dissolved gases exceeds the sum of atmospheric and hydrostatic pressure. Our implementation of ebullition follows that of Tang et al. (2010) and Raivonen et al. (2017), which is a new algorithm based on hydrostatic equilibrium rather than concentration threshold. The ebullition algorithm considers the concentrations of CH_4, O_2, CO_2, H_2, and N_2, when the criterion for bubble formation is reached; such that when

$$\sum_{X} PP_X(z) > P_{atm} + P_{hyd}, \tag{32}$$

ebullition occurs. Here, P_{atm} and P_{hyd} are the atmospheric and hydrostatic pressure (Pa), respectively.

The fraction of ebullition $f_{ebull}(z)$ is calculated as

$$f_{ebull}(z) = \frac{\sum_X PP_X(z) - \left(P_{atm} + P_{hyd}\right)}{\sum_X PP_X(z).} \tag{33}$$

We also use the ebullition rate constant k (d^{-1}) in the equation, so the ebullition rate $Q_{ebull,X}$ (mol m^{-3} d^{-1}) of compound X is calculated as

$$Q_{ebull,X} = k \times \frac{\sigma \times f_{ebull}(z) \times PP_X(z)}{RT}. \tag{34}$$

Here, σ is the porosity, R is the universal gas constant (J mol^{-1} K^{-1}) and T is the soil temperature (K).

The total ebullition flux released into either the atmosphere or soil is determined by water table depth. If the position of the water table is below the soil surface, the bubbles of gas are transported into the overlying air-filled soil layer and are subsequently diffused into the soil or plant aerenchyma. Otherwise, they are directly released into the atmosphere.

The detailed descriptions and baseline values for all parameters of the CH_4 model are listed in Table 1. The algorithms used to describe the dynamics of four microbial groups, the coefficients associated with gas transport processes (including diffusion coefficients, Henry law constants, and Schmidt numbers), and the specific expressions for environmental factors are presented in Appendices A, B, and C, respectively.

3. Data and Methods

3.1. Observations

Continuous observations of CH_4 emissions were compiled from 24 natural wetland sites, covering tropical, temperate, and boreal regions. Detailed information regarding these sites has been reported in previous studies or field work, so site information is briefly introduced in Tables 2–4, including location, wetland types, dominant vegetation, years of observation, and the measurement methods.

3.2. Model Forcing Data

The forcing data for this model mainly include daily climate data, daily water table depth, and soil carbon data. We used the Modern-Era Retrospective Analysis for Research and Applications data set (Gelaro et al., 2017) and the Climate Prediction Center Global Unified Precipitation data provided by the National Oceanic and Atmospheric Administration/Oceanic and Atmospheric Research/Earth System Research Laboratory Physical Sciences Division, Boulder, Colorado, United States (https://www.esrl.noaa.gov/psd/) to drive the model. The Modern-Era Retrospective Analysis for Research and Applications data provided the daily maximum, minimum, and average air temperature, relative humidity, and wind speed at 2 m, and the Climate Prediction Center Global Unified Precipitation data provided the daily precipitation. The soil carbon data for model initialization were obtained from the Global Gridded Surfaces of Selected Soil Characteristics (International Geosphere-Biosphere Programme Data and Information System) data set (Global Soil Data Task Group, 2000), and the soil pH was obtained from the soil properties data set of the Digital Soil Map of the World by Land and Water Development Division, Food and Agriculture Organization (http://www.fao.org/geonetwork/srv/en/metadata.show?id=14116). A spin-up of 200 years

Table 1
Major Parameters in CH_4-Related Processes

Index	Parameter	Value	Range	Units	Descriptions	References
P1	K_{cpool}	0.02	0.0001–0.02		Ratio of dissolved organic carbon to soil organic carbon	
P2	$V_{DOCprodAce,max}$	0.5	0.3–0.7	mol m^{-3} d^{-1}	Maximum acetate production rate from fermentation	Grant (1998)
P3	$K_{DOCprodAce}$	10.0	5–15	mol m^{-3}	Half saturation coefficient	
P4	$K_{AceprodO2}$	0.04	0.01–0.1	mol m^{-3}	Half saturation coefficient	Kettunen (2003)
P5	$V_{H2prodAce,max}$	0.15	0.01–0.3	mol m^{-3} d^{-1}	Maximum acetate production rate from homoacetogenesis	
P6	$V_{H2prodCH4,max}$	0.15	0.01–0.3	mol m^{-3} d^{-1}	Maximum CH_4 production rate from hydrogenotrophic methanogenesis	Grant (1998)
P7	$V_{Acecons,max}$	0.5	0.3–0.7	mol m^{-3} d^{-1}	Maximum acetate consumption rate by acetoclastic methanogensis	Grant (1998)
P8	$V_{CH4oxid,max}$	0.5	0.3–0.7	mol m^{-3} d^{-1}	Maximum CH_4 oxidation rate	Grant (1999)
P9	$K_{H2prodAce}$	0.01	0.01–0.1	mol m^{-3}	Half saturation coefficient	
P10	$K_{CO2prodAce}$	0.05	0.01–0.1	mol m^{-3}	Half saturation coefficient	
P11	$K_{H2prodCH4}$	0.01	0.01–0.1	mol m^{-3}	Half saturation coefficient	
P12	$K_{CO2prodCH4}$	0.05	0.01–0.1	mol m^{-3}	Half saturation coefficient	
P13	$K_{AceprodCH4}$	0.05	0.01–0.1	mol m^{-3}	Half saturation coefficient	Kettunen (2003)
P14	$K_{CH4prod}$	0.5	0.3–0.7	mol mol^{-1}	CH_4 production ratio	Kettunen (2003)
P15	$K_{CH4oxidCH4}$	0.05	0.01–0.1	mol m^{-3}	Half saturation coefficient	Kettunen (2003)
P16	$K_{CH4oxidO2}$	0.02	0.01–0.1	mol m^{-3}	Half saturation coefficient	Kettunen (2003)
P17	$f_{D,w}$	0.8	0.7–0.9		Reduction factor for diffusion in water-filled peat	Raivonen et al. (2017)
P18	$f_{D,a}$	0.8	0.7–0.9		Reduction factor for diffusion in air-filled peat	Raivonen et al. (2017)
P19	τ	1.5	1–2		Root tortuosity	Stephen et al. (1998)
P20	a_{mA}	0.085	0.01–0.1	m^2 kg^{-1}	Root ending area per root dry biomass	Stephen et al. (1998)
P21	SLA	20	15–25	m^2 kg^{-1}	Specific leaf area	Raivonen et al. (2017)
P22	σ	0.8	0.7–0.9		Peat porosity	Raivonen et al. (2017)
P23	k	0.0001	0.0001–0.0003	d^{-1}	Time constant of ebullition	
P24	K_{aer}	0.1	0.1–0.2	mol m^{-3} d^{-1}	O_2 consume rate from aerobic respiration	
P25	K_{aerDOC}	10.0	5–15	mol m^{-3}	Half saturation coefficient	
P26	K_{aerO2}	0.22	0.01–0.3	mol m^{-3}	Half saturation coefficient	
P27	$DOCprodQ_{10}$	2.5	1–5		Temperature sensitivity of DOC production	Kettunen (2003)
P28	$AceprodQ_{10}$	2.5	1–5		Temperature sensitivity of acetate production	Kettunen (2003)
P29	$CH4prodQ_{10}$	2.5	1–5		Temperature sensitivity of CH_4 production	Kettunen (2003)
P30	$CH4oxidQ_{10}$	2.5	1–5		Temperature sensitivity of CH_4 oxidation	Kettunen (2003)

(repeat the climate data of observed years) was done to obtain the modeled soil temperature and moisture, and the last cycle of observed years was used to simulate the CH_4 emissions. The final output of the model was the daily fluxes of gases between soil and atmosphere.

3.3. Sensitivity Analysis

To characterize the sensitivity of the modeled CH_4 emissions to input parameters (Table 1), the polynomial chaos expansion (PCE)-based Sobol sensitivity indices method was employed to assess the response of model output to changes in parameters. The Sobol indices (Sobol, 1993) are convenient representations of the model sensitivity to its parameters and correspond to the variance-based decomposition that aims to decompose the total variance of the model into the sum of the variances of each input variable or their interactions (Ricciuto et al., 2018; Sudret, 2008; Wang et al., 2016). The PCE is a powerful probabilistic technique that uses the orthogonal stochastic polynomials in the random inputs to provide a functional approximation of the model output (Crestaux et al., 2009; Marelli et al., 2019). The Sobol indices are traditionally computed by Monte Carlo simulation, which makes them difficult to apply with computationally expensive models (Sudret, 2008). Instead, the PCE-based Sobol indices method requires less computational effort and is more applicable for the computationally expensive models (Marelli et al., 2019) and has been applied to some sensitivity studies of parameters in earth system model or land surface model (Ricciuto et al., 2018; Shi et al., 2019). The PCE-based Sobol indices method is briefly introduced as follows:

For an input random vector $X = \{X_1, ..., X_k\}$, the PCE of model output $Y = M(X)$ can be established as

Table 2
Description of Sites in Boreal Regions

No.	Site name	Location	Wetland type	Dominant vegetation	Time	Method	References
1	Zackenberg, Greenland	74°30′N, 21°00′W	Arctic Fen	*Eriophorum scheuchzeri*, *Carex stans*, and *Dupontia psilosantha*	2006–2010	Automatic chamber	Mastepanov et al. (2013)
2	Siikaneva, Finland	61°50′N, 24°12′E	Boreal minerotrophic fen	Sedges, Rannoch rush and Mosses	2005–2015	Eddy covariance	Rinne et al. (2018)
3	Lompolojänkkä, Finland	67°59.8′N, 24°12.5′E	Open, nutrient-rich sedge fen	*Betula nana*, *Menyanthes trifoliata*, *Salix lapponum*, and Carex ssp.	2006–2010	Eddy covariance	Raivonen et al. (2017)
4	Stordalen, Sweden	68°21′N, 19°02′E	Subarctic mire	*Eriophorum angustifolium*	2004–2006	Automatic chamber and eddy covariance	Petrescu et al. (2008)
5	Degero Stormyr, Sweden	64°11′N, 19°33′E	Mixed acid mire	*Eriophorum vaginatum*, *Vaccinium oxycoccos*, *Andromeda polifolia*, and *Scheuchzeria palustris*	1995–1997	Static chamber	Granberg et al. (2001)
6	Lena Samoylov Delta, Russia	72°22′N, 126°30′E	Tundra	Sedges, mosses, and shrubs	2003–2004	Eddy covariance	Wille et al. (2008)
7	Bakchar, Russia	56°51′N, 82°50′E	Open unforested mesotrophic fen	*Eriophorum vaginatum*, *Carex rostrata*, *Carex limosa*, and horse-tail *Equisetum fluviatile*	1999	Static chamber	Friborg et al. (2003)
8	Manitoba, Canada	58°40′N, 93°50′W	Eutrophic fen	Sedges, grasses, and moss	2008–2011	Eddy covariance	Hanis et al. (2013)
9	Athabasca, Canada	54°57′N, 112°28′W	Moderately rich treed fen	Stunted trees, shrub, and mosses	2007	Eddy covariance	Long et al. (2010)
10	Quebec, Canada	53°40′N, 78°10′W	Boreal bog	Lichen, mosses, and shrubs	2012	Eddy covariance	Nadeau et al. (2013)
11	Robinsons, Canada	48°16′N, 58°40′W	Boreal bog	Mosses, lichens, and sedge	2014–2016	Eddy covariance	Wang et al. (2018)

Table 3
Description of Sites in Temperate Regions

No.	Site name	Location	Wetland type	Dominant vegetation	Time	Method	References
1	Daxinganling, China	51°7.92′N, 125°8.22′ E	Intermittently inundated marsh	*Carex meyerian* (#1)[a]	2011–2012	Static chamber	Liu et al. (2015)
		52°56′N, 122°51′E	Permafrost peatland	Shrubs, sedges, and grass (#2)	2012–2013	Eddy covariance	Sun et al. (2018)
2	Sanjiang Plain, China	47°53′N, 133°30′E	Permanently inundated marsh	*Glyceria spiculosa* (#1) and *Deyeuxia angustifolia* (#2)	2011	Static chamber	Sun et al. (2013)
				Carex lasiocarpa, *Glyceria spiculosa*, and *Deyeuxia angustifolia* (#3)	2011	Eddy covariance	
		47°35′N, 133°30′E	Permanently inundated marsh	*Carex lasiocarpa* and *Carex pseudocuraica* (#4)	2012–2013	Eddy covariance	Sun et al. (2018)
3	Luanhaizi, China	37°35′N, 101°20′E	Alpine wetland	*Carex pamirensis* and *Carex alrofusca*	2012–2013	Eddy covariance	Song et al. (2015)
4	Ruoergai, China	32°47′N, 102°32′E	Peatland	*Carex muliensis* (#1) and *Carex meyeriana* (#2)	2001	Static chamber	Ding et al. (2004)
5	Minnesota, United States	47°32′N, 93°28′W	Poor fen	Sphagnum, Carex, and *Scheuchzeria palustris* (#1)	1988–1990	Static chamber	Dise (1993)
		47°30′N, 93°29′W	Peatland	*Sphagnum papillosum*, Carex spp., *Eriophorum chamissonis*, and *Saracenia purpurea* (#2)	2009–2011	Eddy covariance	Olson et al. (2013)
6	Sallies Fen, United States	43°12.5′N, 71°3.5′W	Poor fen	Mosses, shrubs, and sedges	2008–2011	Static chamber	Noyce et al. (2014)
7	Michigan, United States	42°27′N, 84°01′W	Ombrotrophic peatland	Sphagnum and *Scheuchzeria palustris*	1991–1993	Static chamber	Shannon and White (1994)
8	Mer Bleue, Canada	45°41′N, 75°52′W	Temperate ombrotrophic bog	Chamaedaphne (#1), Eriophorum (#2), and Maianthemum (#3)	2009–2010	Triplicate auto chamber	Lai et al. (2014)
				Sphagnum spp., Ericaceous shrubs, and Judd. Sedges (#4)	2011–2012	Eddy covariance	Brown et al. (2014)
9	Federseemoor, Germany	48°06′N, 9°38′E	Minerotrophic peatland	Phragmites	2013	Eddy covariance	van den Berg et al. (2016)
10	Schechenfilz, Germany	47°48′N, 11°19′E	Temperate bog-pine forest	Bog-pines and mosses	2012–2013	Eddy covariance	Hommeltenberg et al. (2014)
11	Kopytkowo, Poland	53°35′N, 22°53′E	Temperate mire	Reeds, sedges, and rushes	2013–2014	Eddy covariance	Fortuniak et al. (2017)
12	Kopuatai, New Zealand	37°56′S, 175°22′E	Ombrotrophic, raised bog	Wire rush and *Empodisma robustum*	2012–2014	Eddy covariance	Goodrich et al. (2015)

[a]The observed site with corresponding dominant vegetation.

Table 4
Description of Sites in Tropical Regions

No.	Site name	Location	Wetland type	Dominant vegetation	Time	Method	References
1	Sarawak, Malaysia	1°25′N, 111°07′E	Tropical peat swamp forest	*Gonstylus bancanus*, *Dactylocladus stenostachys*, and *Copaifera palustris* (#1)	2012–2015	Closed chamber	Sangok et al. (2017)
		1°27′N, 111°09′E	Tropical peat swamp forest	*Shorea albida*, *Gonystylus bancanus*, and Stemonurus spp. (#2)	2013	Eddy covariance	Tang et al. (2018)
				Shorea albida, Lithocarpus sp., Litsea sp., and Dillenia sp. (#3)	2014–2015	Eddy covariance	Wong et al. (2018)

$$Y = M(X) = \sum_{\alpha \in \mathbb{N}^k} \lambda_\alpha \Psi_\alpha(X). \tag{35}$$

Here, the $\Psi_\alpha(X)$ are multivariate polynomials orthonormal with regard to the distribution of X, $\alpha \in \mathbb{N}^k$ is an indices vector that identifies the components of the multivariate polynomials Ψ_α, and the $\lambda_\alpha \in \mathbb{R}$ represent the corresponding coefficients.

The sum in equation 35 needs to be truncated to a finite sum, when applied in realistic situation, by the truncated PCE.

$$M(X) \approx M^{PC}(X) = \sum_{\alpha \in A} \lambda_\alpha \Psi_\alpha(X) \tag{36}$$

Here, $A \in \mathbb{N}^k$ is the set of selected multi-indices of multivariate polynomials.

Therefore, when the model $M(X)$ is approximated by the PCE surrogate, the Sobol indices can be computed by its coefficients λ_α as follows:

$$E(M(X)) \approx \lambda_0, \tag{37}$$

$$V(M(X)) \approx \sum_{\substack{\alpha \in A \\ \alpha \neq 0}} \lambda_\alpha^2, \tag{38}$$

$$S_i = \frac{1}{V(M(X))} \sum_{\alpha \in A_{S_i}} \lambda_\alpha^2 \text{ with } A_{S_i} = \{\alpha : \alpha_i > 0, \alpha_k = 0 \text{ for } k \neq i\}, \tag{39}$$

$$S_{Ti} = \frac{1}{V(M(X))} \sum_{\alpha \in A_{S_{Ti}}} \lambda_\alpha^2 \text{ with } A_{S_{Ti}} = \{\alpha : \alpha_i > 0\}, \tag{40}$$

$$S_{ij} = \frac{1}{V(M(X))} \sum_{\alpha \in A_{S_{ij}}} \lambda_\alpha^2 \text{ with } A_{S_{ij}} = \{\alpha : \alpha_i > 0, \alpha_j > 0, \alpha_k = 0 \text{ for } k \neq i, j\}. \tag{41}$$

Here, $E(M(X))$ and $V(M(X))$ indicate the expectation and variance of $M(X)$. S_i, S_{Ti}, and S_{ij} are the first-order Sobol indices, the total Sobol indices, and the second-order Sobol indices (also called the joint Sobol indices), respectively. A_{S_i}, $A_{S_{Ti}}$, and $A_{S_{ij}}$ are the sets of indices vectors that only include the interest term corresponding to the sensitivity index.

The first-order Sobol indices measure the fraction of the variance contributed by the *i*th parameter only; the total Sobol indices measure the total variance contribution due to the *i*th parameter and its interactions with other parameters; and the second-order Sobol indices measure the fractional variance contribution corresponding to the joint *i*th and *j*th parameter (Ricciuto et al., 2018).

3.4. Model Evaluation

Three metrics were used to evaluate model performance, including:

1. The coefficient of determination (R^2), which represents the variation in the observations interpreted by the model.
2. Root mean square error (RMSE), calculated as

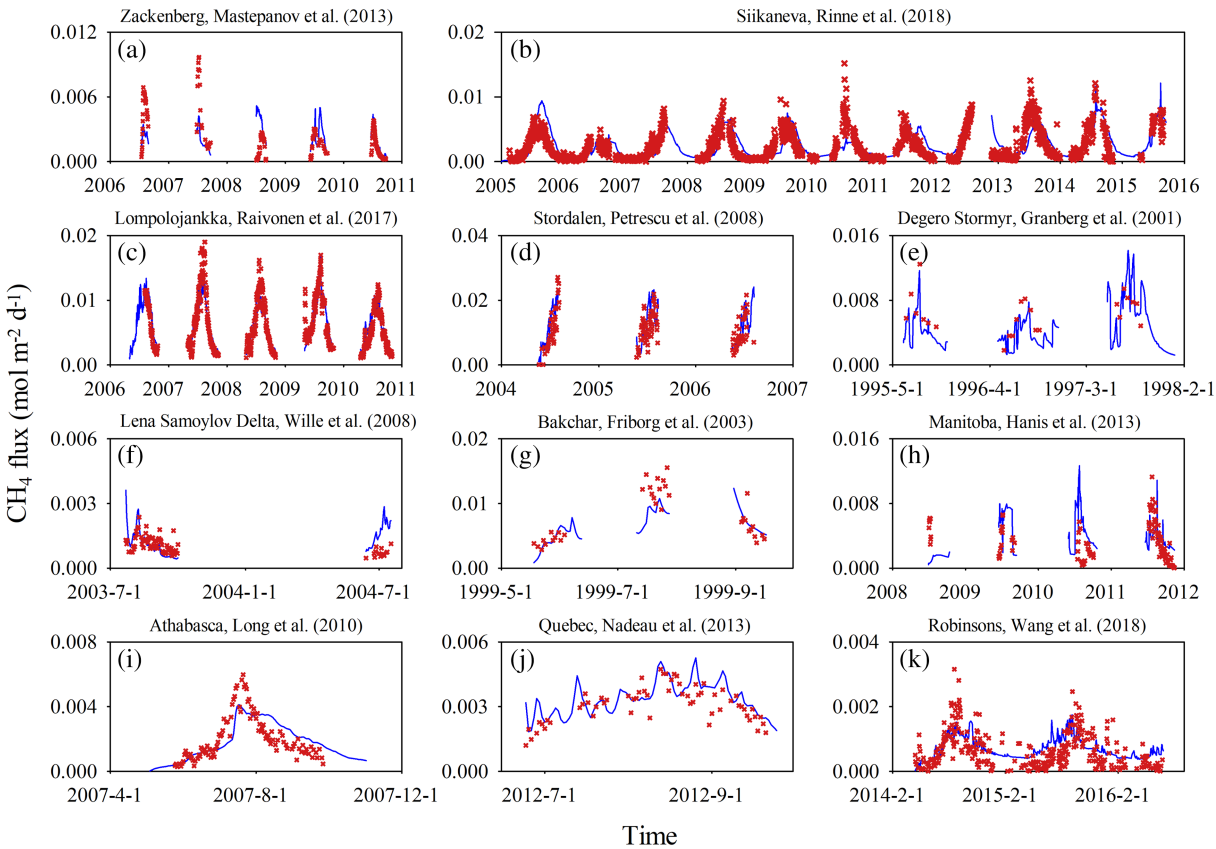

Figure 2. Daily variation in simulated and observed CH_4 emissions at boreal sites. The blue solid lines represent simulated values, and the red cross dots represent observed values.

$$\mathrm{RMSE} = \sqrt{\frac{\sum_{i=1}^{n} (\mathrm{M}_i - \mathrm{O}_i)^2}{n}}. \tag{42}$$

Here, M_i is the modeled value and O_i the observed value; n is the number of days for which we have the observed values.

3. Relative predictive error (RPE), computed as

$$\mathrm{RPE} = \frac{\overline{\mathrm{M}} - \overline{\mathrm{O}}}{\overline{\mathrm{O}}} \times 100\%. \tag{43}$$

Here, $\overline{\mathrm{M}}$ and $\overline{\mathrm{O}}$ are the means of modeled and observed values, respectively.

4. Results

4.1. Model Evaluation

Twenty-four sites were selected to evaluate the CH_4 model (Tables 2–4). These evaluation sites spanned from boreal to tropical regions and covered several dominant wetland types including fen, bog, mire, marsh, peatland swamp, and tundra. We examined model performance by assessing its ability to accurately reproduce the magnitude and temporal variability of CH_4 emissions among these sites.

4.1.1. Boreal Sites

Observations from 11 sites in boreal regions, mainly located in northern Europe and Canada, were compiled for model evaluation, comprising six fen sites, two bog sites, two mire sites, and one tundra site. Overall, the model reliably predicted the observations (Figure 2), with the RPE varying from −19.47% to 33.28% (Table 5).

Table 5
Statistic Results for Site-Level Evaluation

Site	R^2	RMSE[a]	RPE (%)	N
Boreal sites				
Zackenberg	0.210	0.0019	−1.39	192
Siikaneva	0.517	0.0017	14.54	2285
Lompolojänkkä	0.815	0.0018	2.80	837
Stordalen	0.317	0.0057	17.38	126
Degero Stormyr	0.361	0.0028	−19.47	23
Lena Samoylov Delta	0.053	0.0007	15.95	79
Bakchar	0.586	0.0028	−16.55	35
Manitoba	0.012	0.0030	30.08	127
Athabasca	0.563	0.0010	4.38	103
Quebec	0.455	0.0007	10.76	61
Robinsons	0.313	0.0006	33.28	329
Temperate sites				
Daxinganling1	0.297	0.0005	12.31	38
Daxinganling2	0.272	0.0002	15.38	242
Sanjiang1	0.258	0.0030	13.46	54
Sanjiang2	0.000	0.0025	−2.79	57
Sanjiang3	0.379	0.0032	−6.27	119
Sanjiang4	0.413	0.0027	7.04	142
Luanhaizi	0.170	0.0025	−26.70	133
Ruoergai1	0.118	0.0029	20.29	35
Ruoergai2	0.059	0.0039	−19.26	35
Minnesota1	0.689	0.0057	−9.13	54
Minnesota2	0.506	0.0033	4.22	644
Sallies Fen	0.240	0.0052	−28.70	80
Michigan	0.142	0.0147	−27.30	62
Mer Bleue1	0.083	0.0018	−0.19	194
Mer Bleue2	0.498	0.0034	−13.63	208
Mer Bleue3	0.231	0.0028	−28.99	185
Mer Bleue4	0.000	0.0012	−22.68	276
Federseemoor	0.252	0.0043	−3.55	253
Schechenfilz	0.231	0.0012	32.64	145
Kopytkowo	0.145	0.0060	−48.62	239
Kopuatai	0.001	0.0041	−4.97	124
Tropical sites				
Sarawak1	0.016	0.0003	47.04	33
Sarawak2	0.003	0.0010	25.08	61
Sarawak3	0.426	0.0005	6.25	18

[a]The unit of RMSE is mol m^{-2} d^{-1}.

The magnitude and seasonality of simulated CH_4 emissions were consistent with the observations, especially at the Siikaneva and Lompolojänkkä sites (Figures 2b and 2c). Long-term continuous CH_4 observations had been collected at these two sites, and the values of the coefficient of determination (R^2) were about 0.52 and 0.82, respectively (Table 5).

Although the model explained variability in CH_4 emissions well at most sites, large differences between simulated and observed CH_4 emissions were still observed to exist. The model underestimated CH_4 observations at the Zackenberg site; the discrepancies between modeled and observed values mainly occurred in the growing seasons of 2006 and 2007 (Figure 2a). Meanwhile, the model had slight high predicted values in the growing season of 2004 at Lena Samoylov Delta (Figure 2f). At these two sites, R^2 was very low with values of 0.21 and 0.053, respectively (Table 5). In addition, the model predicted slightly lower values for peak emissions at the Bakchar, Athabasca, and Robinsons sites (Figures 2g, 2i, and 2k). The lowest R^2 was produced at the Manitoba site, which simultaneously had a high RPE value (R^2 = 0.012, RPE = 30.08%) (Table 5), indicating that the model failed to capture the variation and magnitude of CH_4 observations at this site.

4.1.2. Temperate Sites

CH_4 flux observations from 12 sites in temperate regions were compiled for model evaluation. On the whole, the model predictions matched the observations well (Figure 3). At the Minnesota and Mer Bleue sites (Figures 3e1, 3e2, and 3h2), the model explained about 69%, 51%, and 50% of the variation observed in CH_4 emissions, respectively (Table 5). The RPE ranged from −28.99% to 32.64%, except at the Kopytkowo site, demonstrating that a lower deviation between simulated and observed CH_4 emissions existed at most sites (Table 5).

However, large differences also existed between modeled and observed CH_4 emissions at some sites. At the Sanjiang sites, the simulated peak emissions clearly lagged the observed peak values (Figures 3b1–3b3). Although they had lower RPEs, with values of 13.46%, −2.79%, and −6.27%, respectively (Table 5), the model predicted little of the variability in observed CH_4 emissions, with R^2 being 0.258, 0.000, and 0.379, respectively (Table 5). At the Ruoergai and Federseemoor sites, observed CH_4 fluxes had no general seasonal patterns (Figures 3d1, 3d2, and 3i). The R^2 values were 0.118, 0.059, and 0.252, and the RMSE values were 0.0029, 0.0039, and 0.0043 mol m^{-2} d^{-1}, respectively (Table 5). Thus, the simulated results only matched the magnitude of observed CH_4 emissions at these two sites. The model underestimated observed CH_4 emissions at the Daxinganling, Minnesota, Michigan and Mer Bleue sites (Figures 3a2, 3e2, 3g, and 3h4), which mainly occurred in the 2013 growing season at Daxinganling, 2011 at Minnesota, 1991 at Michigan, and 2011 at Mer Bleue. Meanwhile, the model slightly overestimated CH_4 emissions at Daxinganling and Mer Bleue in 2012 (Figures 3a2 and 3h4). In addition, the model showed poor agreement between simulated and observed CH_4 emissions at the Luanhaizi, Kopytkowo, and Kopuatai sites (Figures 3c, 3k, and 3l). The calculated R^2 and RPE values at these sites were 0.17 and −26.70%, 0.145 and −48.62%, and 0.001 and −4.97%, respectively (Table 5). At the Kopytkowo site, the model significantly underestimated observations during the growing season in 2013 (Figure 3k).

4.1.3. Tropical Sites

Observations from a tropical peat swamp forest located in Sarawak, Malaysia were also collected for comparison. Overall, the model showed good agreement between simulated CH_4 emissions and observations at this site (Figure 4). At the Sarawak1 site, the simulated CH_4 emissions did not reproduce the variation in observations, which had no clear seasonal patterns (Figure 4a1). In addition, the model slightly overestimated the

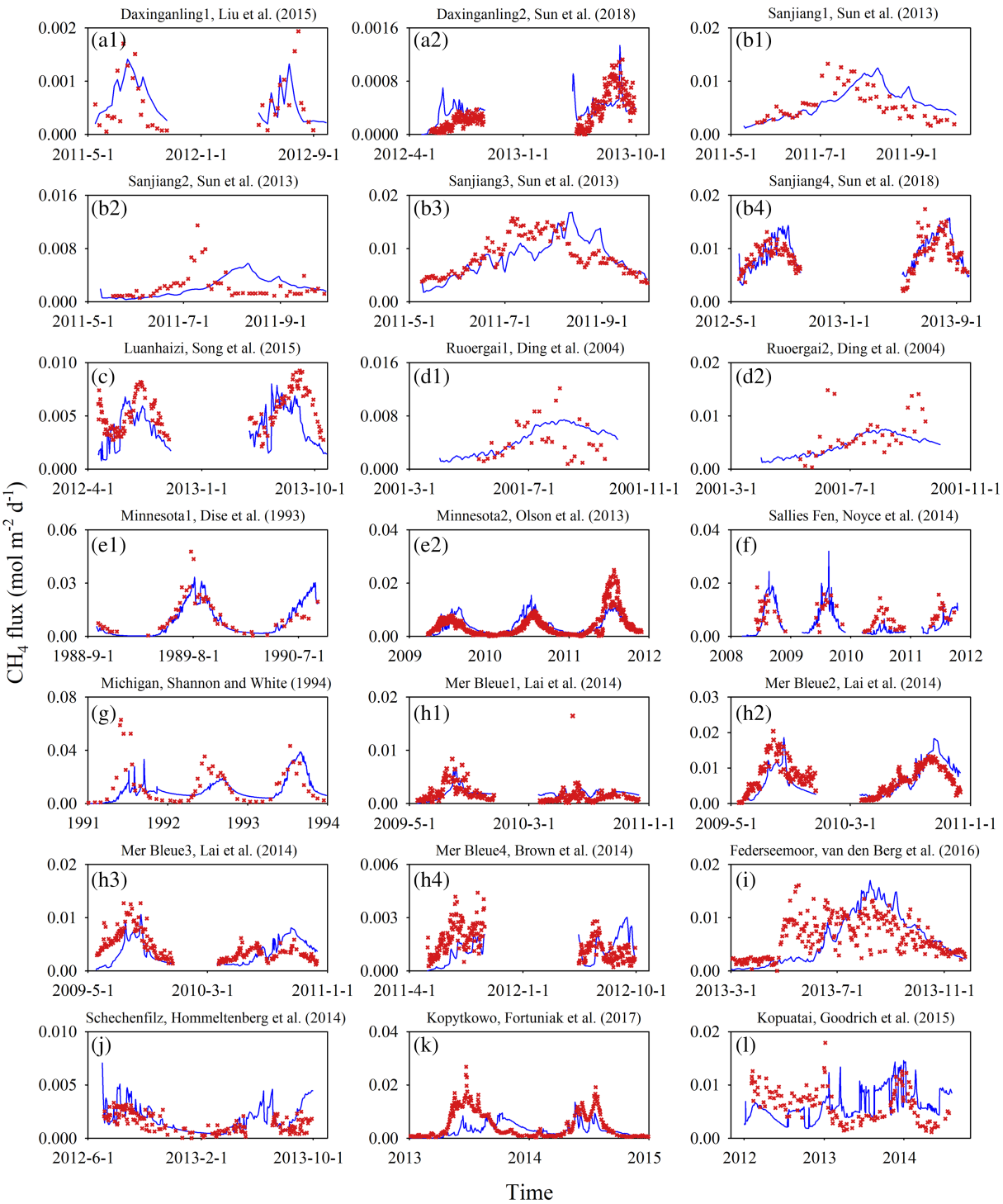

Figure 3. Daily variation in simulated and observed CH_4 emissions at temperate sites. The blue solid lines represent simulated values, and the red cross dots represent observed values.

observed CH_4 emissions in November at the Sarawak2 site (Figure 4a2). The R^2 and RPE values for these two sites were 0.016 and 47.04% and 0.003 and 25.08%, respectively (Table 5). The model captured the magnitude and variation of CH_4 emissions during the measured period at the Sarawak3 site (Figure 4a3). The R^2 and RPE values for this site were 0.426 and 6.25%, respectively (Table 5). The RMSE values for this peat

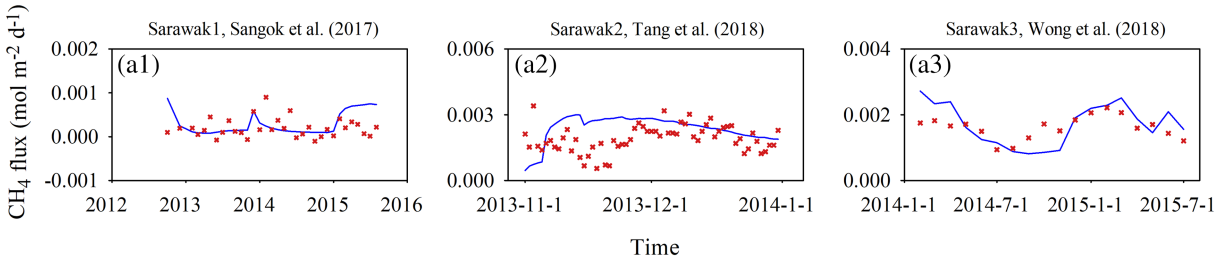

Figure 4. Daily variation in simulated and observed CH_4 emissions at a tropical site. The blue solid lines represent simulated values, and the red cross dots represent observed values.

swamp forest site ranged from 0.0003 to 0.001 mol m^{-2} d^{-1} (Table 5), indicating a small disparity between simulated and observed CH_4 emissions.

The average simulated and observed CH_4 emissions during measured periods for all evaluated, boreal and temperate sites are shown in Figure 5. On the whole, the average values of simulations and observations at all evaluated sites lie close to the 1:1 line over a range of 0 to 0.017 mol m^{-2} d^{-1}, and R^2 is 0.87 (Figure 5a).

4.2. Sensitivity Analysis

The PCE-based parameter sensitivity analysis of modeled CH_4 emissions with 500 model evaluations was performed at seven measured sites, covering the tropical, temperate, and boreal biomes (Figures 6 and 7). For the Siikaneva, Lompolojänkkä, and Quebec sites, $CH4prodQ_{10}$ (P29) is the most sensitive parameter for CH_4 emissions (Figure 6a), which is also reflected in the evaluation of total Sobol indices (Figure 6b).

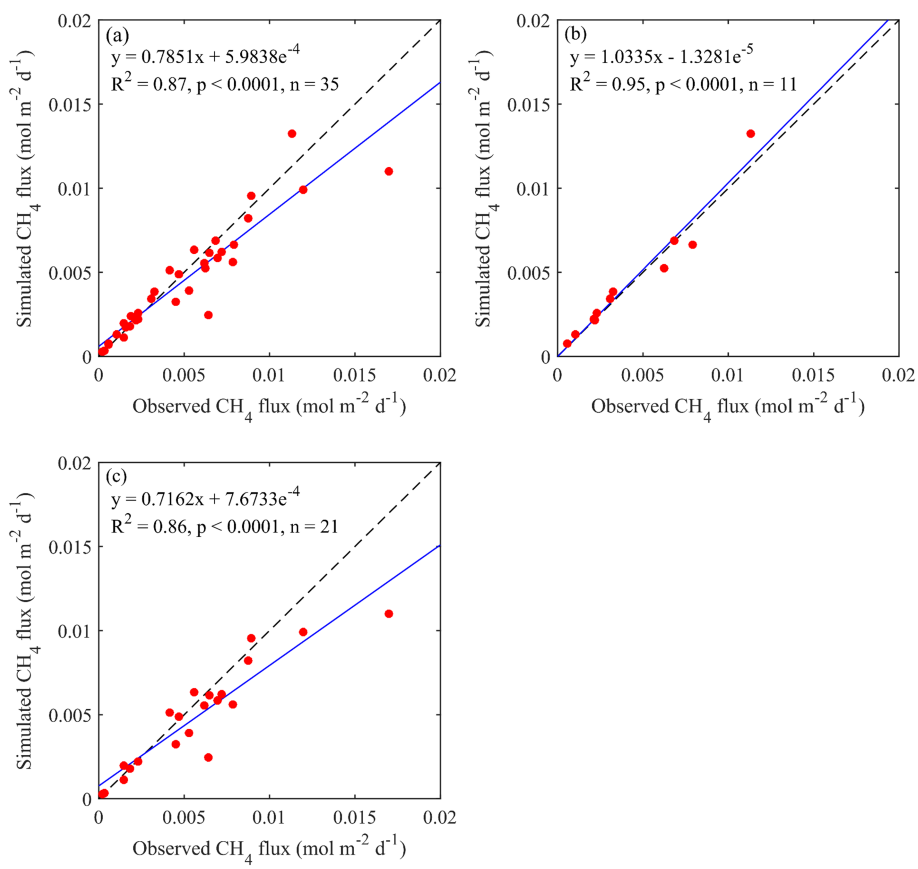

Figure 5. Comparison of the average observed and simulated CH_4 emissions (red dots). (a) All evaluated sites, (b) boreal sites, and (c) temperate sites.

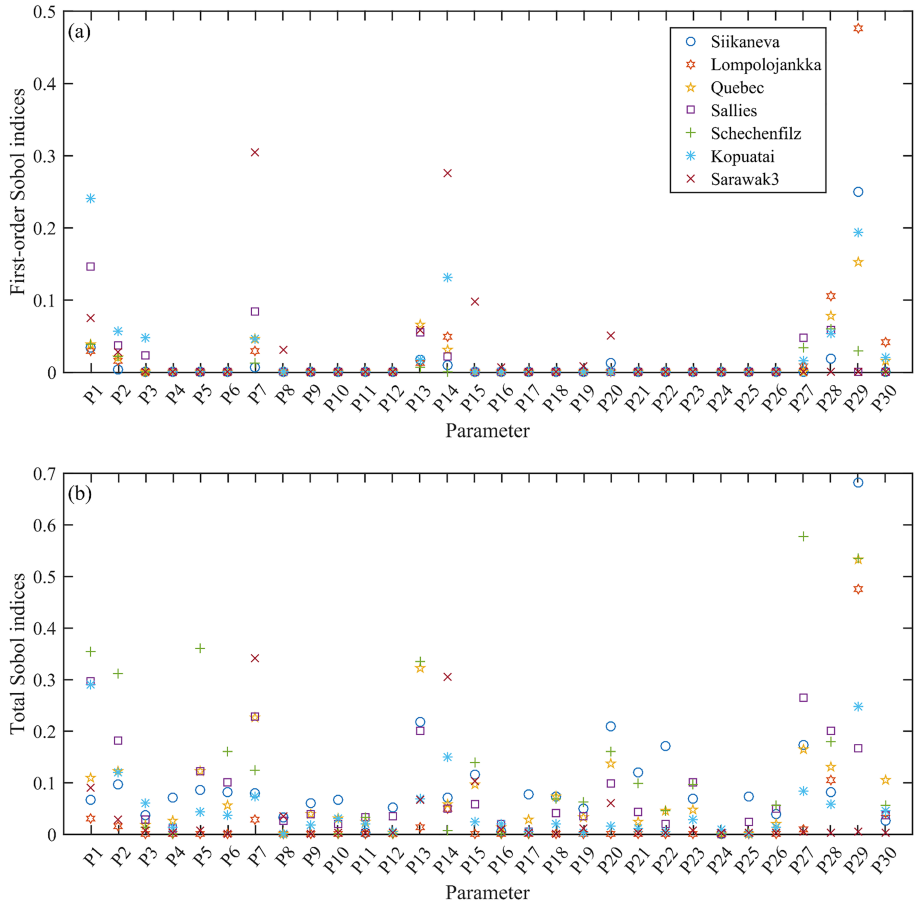

Figure 6. Parameter sensitivity indices for modeled CH_4 emissions. (a) First-order Sobol indices and (b) total Sobol indices. All parameters are listed in Table 1.

For the Sallies and Kopuatai sites, K_{cpool} (P1) has the largest impact on CH_4 emissions (Figures 6a and 6b). In addition, The CH_4 emissions are also sensitive to $V_{Acecons,max}$ (P7), $K_{AceprodCH4}$ (P13), and $DOCprodQ_{10}$ (P27) at the Sallies site and sensitive to $K_{CH4prod}$ (P14) and $CH4prodQ_{10}$ at the Kopuatai site (Figures 6a and 6b). For the Schechenfilz site, the first-order Sobol indices are low for all parameters (Figure 6a). However, the $DOCprodQ_{10}$ has a great total effect index of about 58% on the total variance of CH_4 emissions (Figure 6b), which indicates the apparent impact of this parameter on the CH_4 emissions. For the Sarawak3 site, except for $V_{Acecons,max}$ and $K_{CH4prod}$, the first-order and total Sobol indices have low values for other parameters (Figures 6a and 6b). CH_4 emissions at this site are obviously sensitive to these two parameters, with $V_{Acecons,max}$ becoming the most sensitive parameter (Figures 6a and 6b). Moreover, compared to other sites, the Sobol indices of parameters related to temperature sensitivity (P27–P30) are very low at the Sarawak3 site, which may be related to the high and relatively constant soil temperature in the tropics.

The second-order Sobol indices results indicate that $K_{AceprodCH4}$ and $CH4prodQ_{10}$ have the largest interaction effects on CH_4 emissions at the Siikaneva, Lompolojänkkä, Quebec, Schechenfilz, and Kopuatai sites (Figure 7). The parameters $V_{Acecons,max}$ and $K_{AceprodCH4}$ have the largest interaction effects on CH_4 emissions at the Sallies site, and $V_{Acecons,max}$ and $K_{CH4prod}$ have the largest interaction effects on CH_4 emissions at the Sarawak3 site (Figure 7). In addition, $V_{Acecons,max}$ and $CH4prodQ_{10}$ have the important interaction effects on CH_4 emissions at the Siikaneva, Lompolojänkkä, and Quebec sites (Figure 7). For the Lompolojänkkä site, the parameter subset of $AceprodQ_{10}$ and $CH4prodQ_{10}$ also has the important interaction effects on CH_4 emissions (Figure 7). The parameter set of K_{cpool} and $V_{Acecons,max}$ and the parameter set of $V_{Acecons,max}$ and $AceprodQ_{10}$ also have the important interaction effects on CH_4 emissions at the Sallies site (Figure 7).

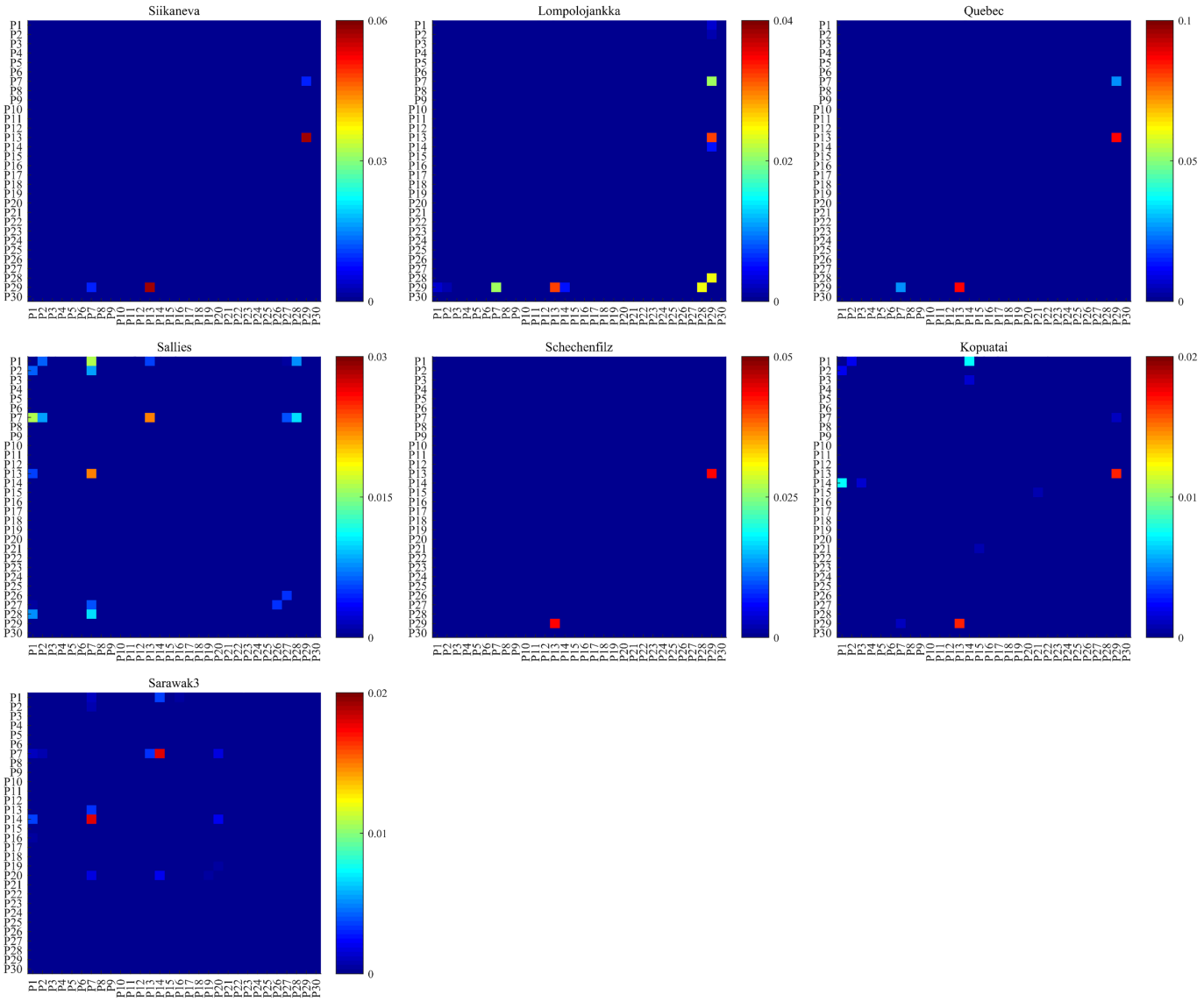

Figure 7. The second-order Sobol indices for modeled CH_4 emissions. All parameters are listed in Table 1.

Although the results of first-order, total, and second-order Sobol indices among the parameters are somewhat different between these sites, the main sensitivity parameters are $DOCprodQ_{10}$, $AceprodQ_{10}$, $CH4prodQ_{10}$, K_{cpool}, $V_{Acecons,max}$, $K_{AceprodCH4}$, and $K_{CH4prod}$, which indicates that these parameters that control DOC and acetate production and acetoclastic methanogenesis have the significant impact on modeled CH_4 emissions.

4.3. Environmental Controls on CH_4 Emissions

At the above test sites, inconsistent relationships between simulated CH_4 emissions, soil temperature, and measured water table position were observed (Figure S1). For example, the seasonality of simulated CH_4 emissions at the Siikaneva and Lompolojänkkä sites depended on soil temperature dynamics and had no significant correlation with water table position. However, at the Sarawak3 site, the temporal variation of simulated CH_4 emissions coincided well with water table position but showed no dependence on soil temperature. In addition, combined effects of soil temperature and water table position were observed on simulated CH_4 emissions at other sites. The soil temperature and water table position exerted a positive effect on simulated CH_4 emissions during the growing season at the Quebec site, where peak emissions

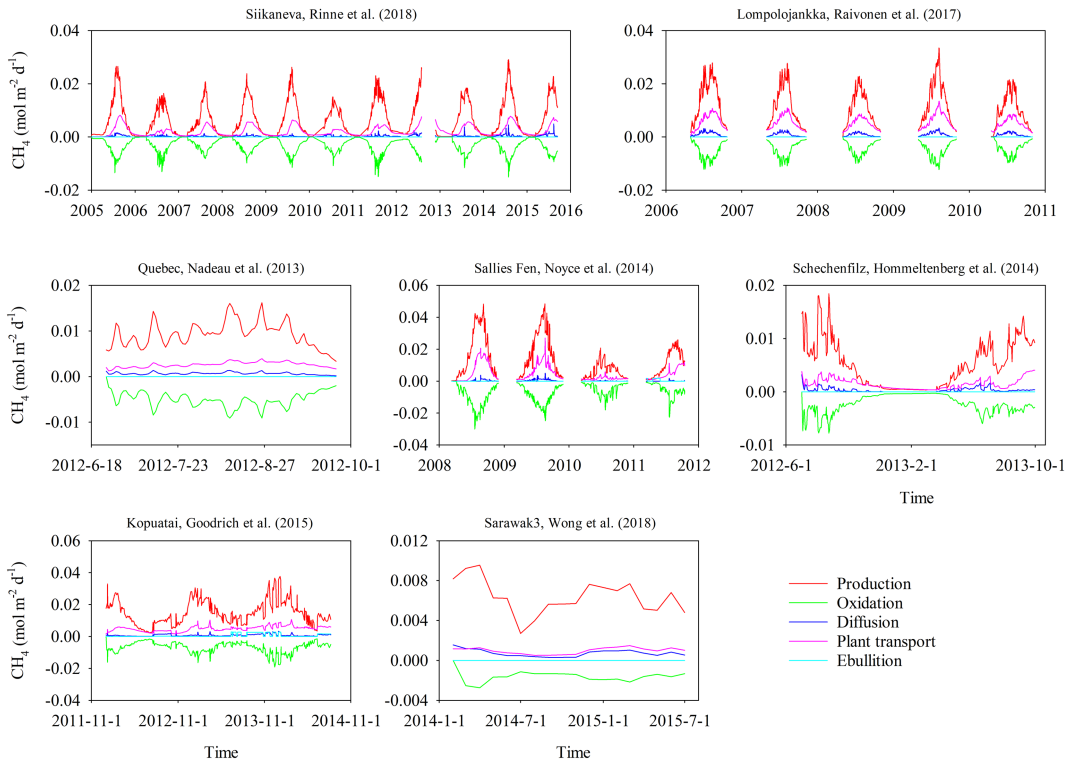

Figure 8. Time series of simulated CH_4 production, oxidation, and transportation.

occurred when soil temperature and water table position reached their maximum. However, although soil temperature had a positive effect at the other sites, an increase of water table position had little influence on simulated CH_4 emissions, and a decrease substantially reduced CH_4 emissions, especially during the growing season.

5. Discussion

5.1. Modeled Process Components

The new CH_4 model explicitly represented CH_4-related microbial mechanisms, including anaerobic fermentation, homoacetogenesis, hydrogenotrophic methanogenesis, acetoclastic methanogenesis, and methanotrophy, and the interaction of different gases, including CH_4, O_2, CO_2, and H_2, in wetland CH_4 emission modeling. The new model has also been integrated into a terrestrial ecosystem model (IBIS) and evaluated at 24 different wetland sites globally. The simulated results captured the magnitude and variation of observed CH_4 emissions at most sites.

Net CH_4 emission is determined by the CH_4 production by methanogens, CH_4 oxidation by methanotrophs, and molecular diffusion, plant-mediated transport, and ebullition to the atmosphere (Chanton, 2005). To assess these processes represented by the model, we calculated the temporal variation in process components of wetland CH_4 emissions at the test sites (Figure 8) and the proportion that each process relative to CH_4 production at all evaluated sites (Figure 9).

Methanotrophy is an important process and can be up to 100% of CH_4 production (Fritz et al., 2011; Whalen, 2005). An almost completely CH_4 oxidation in a densely rooted bog has been reported recently from an analysis of isotopic $\delta^{13}C$-CH_4 values (e et al., 2019). The CH_4 oxidation of global wetland has also been estimated to be 40–70% of total CH_4 production (Megonigal et al., 2004). In our results, CH_4 production and oxidation showed apparent temporal variation at all test sites, with peak values of both processes occurring in the midgrowing seasons (Figure 8). This may reflect enhanced microbial activities caused by the high

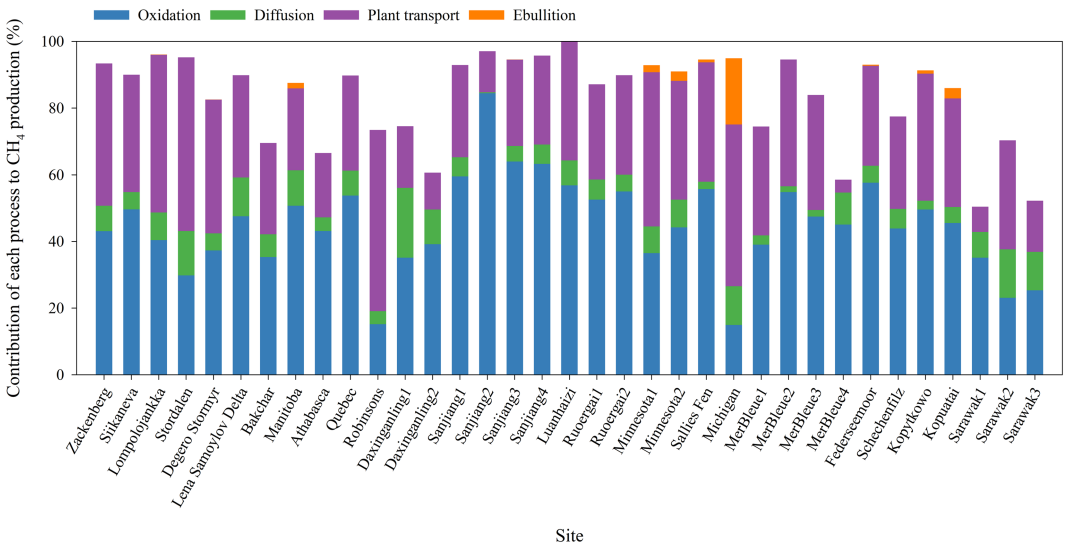

Figure 9. Simulated contributions (%) of CH_4 oxidation, diffusion, plant transport, and ebullition processes to CH_4 production (which is set to 100%); the rest is left in the soil.

temperature in this period (Dunfield et al., 1993). In addition, at all evaluated sites, CH_4 oxidation was observed to be about half or more of CH_4 production (Figure 9).

Plant-mediated transport has been reported as the principal pathway for CH_4 emissions (Colmer, 2003; Green & Baird, 2012; King et al., 1998; Waddington et al., 1996; Whiting & Chanton, 1992). In our analysis, plant-mediated transport also showed clear temporal variation and played a primary role in total observed period, followed by molecular diffusion, and ebullition had the smallest contribution and being characterized by pulse behavior (Figure 8). Moreover, plant-mediated transport also had the greatest proportion of total CH_4 emission at most sites (Figure 9).

5.2. Environmental Controls on CH_4 Emissions

Numerous studies have identified soil temperature as the fundamental control on wetland CH_4 emissions (Liu et al., 2015; Rinne et al., 2018; Sun et al., 2018), with an exponential dependence of CH_4 emissions on soil temperature being recorded (Marushchak et al., 2016; Mikhaylov et al., 2015). Water table position is also generally recognized as a major physical control on CH_4 emissions from wetlands (Moore et al., 2011; Wong et al., 2018). The relationship between water table position and CH_4 emissions is usually nonmonotonic (Brown et al., 2014; Christensen et al., 2003). However, several studies have reported no significant dependence of CH_4 emissions on water table position (Jackowicz-Korczyński et al., 2010; Liu et al., 2015; Rinne et al., 2018). In addition, combined effects of soil temperature and water table position are observed on CH_4 emissions from wetlands (Goodrich et al., 2015; Lai et al., 2014; Noyce et al., 2014).

This study analyzed the relationships between modeled CH_4 emissions and soil temperature and observed water table position at seven test sites. The different control patterns of these two variables on observed CH_4 emissions are reflected in our simulations (see section 3.3). At the Lompolojänkkä site, the water table position is almost always above the soil surface (Figure S1); this may maintain a relatively stable environment for wetland CH_4 dynamics. Thus, the water table position had little or no effect on CH_4 emissions, which was also observed in continuously inundated ecosystems (Strachanm et al., 2015; Sturtevant et al., 2016; Sun et al., 2013). The seasonal variation of simulated CH_4 emissions at the Siikaneva site was controlled by soil temperature (Figure S1), which was consistent with the analysis of observations (Rinne et al., 2018). For the opposite control pattern on simulated CH_4 emissions at the Sarawak3 site (Figure S1), which may be due to the high and narrow range of soil temperature in tropical regions (Hirano et al., 2014; Melling et al., 2005).

5.3. Model Limitations

Comparing to site-level observations inevitably leads to differences and occasionally substantial deviations. Our evaluation identified large differences between modeled and observed CH_4 emissions at some sites. An interpretation for the differences between predictions and observations is the inadequacy of model algorithms. Although we used several microbial mechanisms to represent CH_4 production and oxidation, no observations can be acquired at the site level to evaluate these microbial dynamics, which needs to be improved in the future (Allison et al., 2010). Ebullition is an episodic and complex process that depends on the total partial pressure of dissolved gases and atmospheric and hydrostatic pressure (Tokida et al., 2007). Although we adopted the hydrostatic equilibrium-based algorithm to describe this process, the modeled ebullition may also contribute to the differences to reproduce the observed CH_4 emissions, especially for peak values (Wania et al., 2010).

The gridded inputs play an important role in the prediction at regional and global scales, while local environmental conditions may differ significantly, especially for the meteorological conditions (Wania et al., 2010). Deviations in these conditions will be added into the simulation of vegetation production and soil hydrothermal dynamics and so will propagate into the CH_4 biogeochemical modeling (Riley et al., 2011). Moreover, the coarse time resolution of daily meteorological values may not capture the sharp changes accurately in the processes related to CH_4 emissions, like ebullition. Thus, the uncertainties from forcing data may also contribute to the differences between predictions and observations.

The performance of this new model is comparable with other models. Raivonen et al. (2017) developed a CH_4 emission model of peatland soils (HelsinkI Model of MEthane buiLd-up and emission, HIMMELI) and evaluated at the Siikaneva site. Overall, HIMMELI model showed the coefficient of determination (R^2) between observations and / of 0.63 at the Siikaneva site, which are comparable with our model of 0.52 (Table 5). Wania et al. (2010) evaluated the performance of LPJ-WHyMe (Lund-Potsdam-Jena Wetland Hydrology and Methane) at seven sites, and three of seven sites also are included in our model evaluation (i.e., Michigan, Minnesota, and Ruoergai). The RMSE of LPJ-WHyMe at these three sites range from 0.0011 to 0.014 mol m^{-2} d^{-1} using global parameters, and the RMSE of our model are quite close with them (0.0029 to 0.0147 mol m^{-2} d^{-1}) (Table 5).

Continuous observation and modeling work should be conducted to improve our knowledge of wetland CH_4 dynamics. It is necessary to measure multiple gases at different temporal and spatial scales and separate their different transport pathways (Bridgham et al., 2013). For those areas with sparse observations, such as the tropics, more extensive measurements are particularly needed. Soil carbon and hydrothermal dynamics are important for CH_4 biogeochemical modeling (Kaiser et al., 2017). Although both have been integrated into terrestrial ecosystem models, the improvement of these processes, especially the modeling of water table dynamics, should be made at the fine scale (Zhu et al., 2014). In addition, CH_4 production and oxidation driven by microbes, the important predecessor processes of CH_4 emissions, require further breakthroughs in experiments and observations and should be better to serve to the evaluation of the microbial dynamics (Xu et al., 2016).

6. Conclusions

A new wetland CH_4 emission model was developed and integrated into a terrestrial ecosystem model (IBIS). The new model fully considered CH_4 production, oxidation, and three transport pathways and the interaction between CH_4 and other gases and used four main microbial mechanisms to represent CH_4 production and oxidation. We evaluated the model at 24 globally representative wetland sites. The simulated and observed results showed good agreement for most sites in terms of emission magnitude and variability, and the mean simulated and observed values were highly correlated with an R^2 of 0.87. Sensitivity analysis indicated that those controlling DOC and acetate production and acetoclastic methanogenesis are the main parameters that affect CH_4 emissions. The new process-based model is an attempt to incorporate the microbial mechanisms into the wetland CH_4 emission modeling. In the future, more complete observations and better integration with terrestrial ecosystem models will help to reduce the uncertainties in prediction.

Appendix A: Microbial Dynamics Related to CH_4 Production and Oxidation

Microbial dynamics related to CH_4 production and oxidation are represented by the following equations, which are derived from Kettunen (2003) and Grant (1998):

$$\frac{\partial \text{Homoacetogens}}{\partial t} = \text{Homoacetogens}_{\text{growth}} - \text{Homoacetogens}_{\text{death}}, \tag{A1}$$

$$\frac{\partial \text{H2methanogens}}{\partial t} = \text{H2methanogens}_{\text{growth}} - \text{H2methanogens}_{\text{death}}, \tag{A2}$$

$$\frac{\partial \text{Acemethanogens}}{\partial t} = \text{Acemethanogens}_{\text{growth}} - \text{Acemethanogens}_{\text{death}}, \tag{A3}$$

$$\frac{\partial \text{Methanotrophs}}{\partial t} = \text{Methanotrophs}_{\text{growth}} - \text{Methanotrophs}_{\text{death}}, \tag{A4}$$

where

$$\text{Homoacetogens}_{\text{growth}} = \text{Grow}_{\text{Homoacetogens}} \times 4 \times \text{H2prodAce}, \tag{A5}$$

$$\text{H2methanogens}_{\text{growth}} = \text{Grow}_{\text{H2methanogens}} \times 4 \times \text{H2prodCH4}, \tag{A6}$$

$$\text{Acemethanogens}_{\text{growth}} = \text{Grow}_{\text{Acemethanogens}} \times \text{Acecons}, \tag{A7}$$

$$\text{Methanotrophs}_{\text{growth}} = \text{Grow}_{\text{Methanotrophs}} \times \text{R}_{\text{oxid,CH}_4}, \tag{A8}$$

$$\text{Homoacetogens}_{\text{death}} = \text{Dead}_{\text{Homoacetogens}} \times \text{Homoacetogens} \times f_{T1}, \tag{A9}$$

$$\text{H2methanogens}_{\text{death}} = \text{Dead}_{\text{H2methanogens}} \times \text{H2methanogens} \times f_{T2}, \tag{A10}$$

$$\text{Acemethanogens}_{\text{death}} = \text{Dead}_{\text{Acemethanogens}} \times \text{Acemethanogens} \times f_T(\text{CH4prodQ}_{10}), \tag{A11}$$

$$\text{Methanotrophs}_{\text{death}} = \text{Dead}_{\text{Methanotrophs}} \times \text{Methanotrophs} \times f_T(\text{CH4oxidQ}_{10}). \tag{A12}$$

Here, $\text{Homoacetogens}_{\text{growth}}$ and $\text{Homoacetogens}_{\text{death}}$ are the growth and the death of homoacetogens, respectively; $\text{H2methanogens}_{\text{growth}}$ and $\text{H2methanogens}_{\text{death}}$ are the growth and death of hydrogenotrophic methanogens, respectively; $\text{Acemethanogens}_{\text{growth}}$ and $\text{Acemethanogens}_{\text{death}}$ are the growth and the death of acetoclastic methanogens, respectively; and $\text{Methanotrophs}_{\text{growth}}$ and $\text{Methanotrophs}_{\text{death}}$ are the growth and the death of methanotrophs, respectively. $\text{Grow}_{\text{Homoacetogens}}$, $\text{Grow}_{\text{H2methanogens}}$, $\text{Grow}_{\text{Acemethanogens}}$, and $\text{Grow}_{\text{Methanotrophs}}$ are the growth efficiency for the corresponding microbial functional group, the values of which are 0.2, 0.2, 0.3, and 0.4, respectively; $\text{Dead}_{\text{Homoacetogens}}$, $\text{Dead}_{\text{H2methanogens}}$, $\text{Dead}_{\text{Acemethanogens}}$ and $\text{Dead}_{\text{Methanotrophs}}$ are the death rate (d^{-1}) for the corresponding microbial functional group, whose values are uniformly set to 0.06.

Appendix B: Coefficients Associated With Transportation of Gases.

The diffusivities of four gases in air and water (Tang et al., 2010) are calculated as

$$\text{D}^{\text{air}}_{\text{CH}_4} = 1.9 \times 10^{-5} \times \left(\frac{T}{T_{\varnothing}}\right)^{1.82}, \tag{B1}$$

$$\text{D}^{\text{air}}_{\text{O}_2} = 1.8 \times 10^{-5} \times \left(\frac{T}{T_{\varnothing}}\right)^{1.82}, \tag{B2}$$

$$\text{D}^{\text{air}}_{\text{CO}_2} = 1.47 \times 10^{-5} \times \left(\frac{T}{T_{\varnothing}}\right)^{1.792}, \tag{B3}$$

$$\text{D}^{\text{air}}_{\text{H}_2} = 6.68 \times 10^{-5} \times \left(\frac{T}{T_{\varnothing}}\right)^{1.82}, \tag{B4}$$

$$D_{CH_4}^{water} = 1.5 \times 10^{-9} \times \left(\frac{T}{T_\theta}\right), \tag{B5}$$

$$D_{O_2}^{water} = 2.4 \times 10^{-9} \times \left(\frac{T}{T_\theta}\right), \tag{B6}$$

$$D_{CO_2}^{water} = 1.81 \times 10^{-6} \times \exp\left(\frac{-2,032.6}{T}\right), \tag{B7}$$

$$D_{H_2}^{water} = 5.11 \times 10^{-9} \times \left(\frac{T}{T_\theta}\right). \tag{B8}$$

The Henry's law constant for each gas is computed following Sander (2015), which can be expressed as

$$H_{CH_4} = 1.3 \times 10^{-3} \times \exp\left[1,700 \times \left(\frac{1}{T} - \frac{1}{T_\theta}\right)\right], \tag{B9}$$

$$H_{O_2} = 1.3 \times 10^{-3} \times \exp\left[1,500 \times \left(\frac{1}{T} - \frac{1}{T_\theta}\right)\right], \tag{B10}$$

$$H_{CO_2} = 3.4 \times 10^{-2} \times \exp\left[2,400 \times \left(\frac{1}{T} - \frac{1}{T_\theta}\right)\right], \tag{B11}$$

$$H_{H_2} = 7.8 \times 10^{-4} \times \exp\left[530 \times \left(\frac{1}{T} - \frac{1}{T_\theta}\right)\right]. \tag{B12}$$

Here, T is the soil temperature (K), and $T_\varnothing$ and T_θ are reference temperatures (K) with values of 273.15 and 298, respectively. In here, H_X is expressed in M atm^{-1} and can be converted to mol m^{-3} Pa by multiplying with the conversion factor θ, which value is 9.8623×10^{-3} (Sander, 2015).

The Schmidt number for each gas is calculated following Wania et al. (2010), which can be expressed as

$$Sc_{CH_4} = 1,898 - 110.1 \times T_s + 2.834 \times {T_s}^2 - 0.02791 \times {T_s}^3, \tag{B13}$$

$$Sc_{O_2} = 1,800.6 - 120.1 \times T_s + 3.7818 \times {T_s}^2 - 0.047608 \times {T_s}^3, \tag{B14}$$

$$Sc_{CO_2} = 1,911 - 113.7 \times T_s + 2.967 \times {T_s}^2 - 0.02943 \times {T_s}^3, \tag{B15}$$

$$Sc_{H_2} = 629.95 - 34.691 \times T_s + 0.8681 \times {T_s}^2 - 0.0084 \times {T_s}^3. \tag{B16}$$

Here, T_s is the soil temperature in degree Celsius.

Appendix C: Environmental Controls.

The soil temperature factors are calculated as

$$f_T(Q_{10}) = \begin{cases} 0 & T < 0 \\ Q_{10}^{\frac{T-30}{10}} & 0 \le T \le 30 \\ 1 & T > 30 \end{cases}, \tag{C1}$$

$$f_{T1} = \frac{(T - T_{min1}) \times (T - T_{max1})}{(T - T_{min1}) \times (T - T_{max1}) - (T - T_{opt1})^2}, \tag{C2}$$

$$f_{T2} = \frac{(T - T_{min2}) \times (T - T_{max2})}{(T - T_{min2}) \times (T - T_{max2}) - (T - T_{opt2})^2}. \tag{C3}$$

The soil pH factor is calculated as

$$f_{\mathrm{pH}} = \frac{(\mathrm{pH} - \mathrm{pH}_{\min}) \times (\mathrm{pH} - \mathrm{pH}_{\max})}{(\mathrm{pH} - \mathrm{pH}_{\min}) \times (\mathrm{pH} - \mathrm{pH}_{\max}) - \left(\mathrm{pH} - \mathrm{pH}_{\mathrm{opt}}\right)^2}. \tag{C4}$$

Here, T is the soil temperature (°C); Q_{10} represents the temperature sensitivity in different conditions, including DOCprodQ_{10}, AceprodQ_{10}, CH4prodQ_{10}, and CH4oxidQ_{10}, all of which have a value of 2.5; $T_{\min 1}$ and $T_{\min 2}$ are the minimum soil temperature (°C), whose values are 0 and 20, respectively; $T_{\max 1}$ and $T_{\max 2}$ are the maximum soil temperature (°C), whose values are 20 and 50, respectively; and $T_{\mathrm{opt}1}$ and $T_{\mathrm{opt}2}$ are the optimum soil temperature (°C), whose values are 10 and 35, respectively. pH is the pH value, and $\mathrm{pH}_{\min}$, $\mathrm{pH}_{\max}$, and $\mathrm{pH}_{\mathrm{opt}}$ are the minimum, maximum, and optimum pH, with values of 3, 9, and 6.2, respectively. Soil pH factor was calculated with reference to Cao et al. (1996) and Meng et al. (2012). The soil moisture factor f_{moist} was adopted from the IBIS.

Acknowledgments
The research was funded by the National Key Research and Development Program of China (2016YFA0602701), National Youth Top-Notch Talent Support Program (2015-48), Changjiang Young Scholars Program of China (Q2016161), Fok Ying Tung Education Foundation, and the Fundamental Research Funds for the Central Universities (18lgpy09). The Modern-Era Retrospective Analysis for Research and Applications (MERRA) data set is available at https://gmao.gsfc.nasa.gov/. The CPC Global Unified Precipitation data are available at https://www.esrl.noaa.gov/psd/. The Global Gridded Surfaces of Selected Soil Characteristics (IGBP-DIS) data set is accessible at http://daac.ornl.gov. The soil properties data set of the Digital Soil Map of the World (DSMW) is accessible at http://www.fao.org/geonetwork/srv/en/metadata.show?id=14116. The PCE-based Sobol indices method originated from https://www.uqlab.com/. The CH_4 flux observations evaluated in this paper are collected from the corresponding reference in Table 22–4.

References

Allison, S. D., Wallenstein, M. D., & Bradford, M. A. (2010). Soil-carbon response to warming dependent on microbial physiology. *Nature Geoscience*, *3*, 336–340. https://doi.org/10.1038/ngeo846

Arah, J. R., & Stephen, K. D. (1998). A model of the processes leading to methane emission from peatland. *Atmospheric Environment*, *32*(19), 3257–3264. https://doi.org/10.1016/S1352-2310(98)00052-1

Bohn, T. J., & Lettenmaier, D. P. (2010). Systematic biases in large-scale estimates of wetland methane emissions arising from water table formulations. *Geophysical Research Letters*, *37*, L22401. https://doi.org/10.1029/2010GL045450

Bohn, T. J., Melton, J. R., Ito, A., Kleinen, T., Spahni, R., Stocker, B. D., et al. (2015). WETCHIMP-WSL: Intercomparison of wetland methane emissions models over West Siberia. *Biogeosciences*, *12*(11), 3321–3349. https://doi.org/10.5194/bg-12-3321-2015

Bridgham, S. D., Cadillo-Quiroz, H., Keller, J. K., & Zhuang, Q. L. (2013). Methane emissions from wetlands: Biogeochemical, microbial, and modeling perspectives from local to global scales. *Global Change Biology*, *19*(5), 1325–1346. https://doi.org/10.1111/gcb.12131

Brown, M. G., Humphreys, E. R., Moore, T. R., Roulet, N. T., & Lafleur, P. M. (2014). Evidence for a nonmonotonic relationship between ecosystem-scale peatland methane emissions and water table depth. *Journal of Geophysical Research: Biogeosciences*, *119*, 826–835. https://doi.org/10.1002/2013JG002576

Cao, M., Marshall, S., & Gregson, K. (1996). Global carbon exchange and methane emissions from natural wetlands: Application of a process-based model. *Journal of Geophysical Research*, *101*(D9), 14,399–14,414. https://doi.org/10.1029/96JD00219

Chanton, J. P. (2005). The effect of gas transport on the isotope signature of methane in wetlands. *Organic Geochemistry*, *36*(5), 753–768. https://doi.org/10.1016/j.orggeochem.2004.10.007

Christensen, T. R., Ekberg, A., et al. (2003). Factors controlling large-scale variations in methane emissions from wetlands. *Geophysical Research Letters*, *30*(7), 1414. https://doi.org/10.1029/2002GL016848

Cole, J. J., & Caraco, N. F. (1998). Atmospheric exchange of carbon dioxide in a low-wind oligotrophic lake measured by the addition of SF_6. *Limnology and Oceanography*, *43*(4), 647–656. https://doi.org/10.4319/lo.1998.43.4.0647

Colmer, T. D. (2003). Long distance transport of gases in plants: A perspective on internal aeration and radial oxygen loss from roots. *Plant, Cell & Environment*, *26*(1), 17–36. https://doi.org/10.1046/j.1365-3040.2003.00846.x

Conrad, R. (1999). Contribution of hydrogen to methane production and control of hydrogen concentration in methanogenic soils and sediments. *FEMS Microbiology Ecology*, *28*(3), 193–202. https://doi.org/10.1016/S0168-6496(98)00086-5

Crestaux, T., Le Matre, O., & Martinez, J. (2009). Polynomial chaos expansion for sensitivity analysis. *Reliability Engineering & System Safety*, *94*(7), 1161–1172. https://doi.org/10.1016/j.ress.2008.10.008

Ding, W. X., Cai, Z. C., & Wang, D. X. (2004). Preliminary budget of methane emissions from natural wetlands in China. *Atmospheric Environment*, *38*(5), 751–759. https://doi.org/10.1016/j.atmosenv.2003.10.016

Dise, N. B. (1993). Methane emission from Minnesota peatlands: Spatial and seasonal variability. *Global Biogeochemical Cycles*, *7*(1), 123–142. https://doi.org/10.1029/92GB02299

Dunfield, P., Dumont, R., & Moore, T. R. (1993). Methane production and consumption in temperate and subarctic peat soils, response to temperature and pH. *Soil Biology and Biochemistry*, *25*(3), 321–326. https://doi.org/10.1016/0038-0717(93)90130-4

Foley, J. A., Prentice, I. C., Ramankutty, N., Levis, S., Pollard, D., Sitch, S., & Haxeltine, A. (1996). An integrated biosphere model of land surface processes, terrestrial carbon balance, and vegetation dynamics. *Global Biogeochemical Cycles*, *10*(4), 603–628. https://doi.org/10.1029/96GB02692

Fortuniak, K., Pawlak, W., Bednorz, L., Grygoruk, M., Siedlecki, M., & Zielinski, M. (2017). Methane and carbon dioxide fluxes of a temperate mire in Central Europe. *Agricultural and Forest Meteorology*, *232*, 306–318. https://doi.org/10.1016/j.agrformet.2016.08.023

Friborg, T., Soegaard, H., Christensen, T. R., Lloyd, C. R., & Panikov, N. S. (2003). Siberian wetlands: Where a sink is a source. *Geophysical Research Letters*, *30*(21), 2129. https://doi.org/10.1029/2003GL017797

Fritz, C., Pancotto, V. A., Elzenga, J. T. M., Visser, E. J. W., Grootjans, A. P., Pol, A., et al. (2011). Zero methane emission bogs: Extreme rhizosphere oxygenation by cushion plants in Patagonia. *The New Phytologist*, *190*(2), 398–408. https://doi.org/10.1111/j.1469-8137.2010.03604.x

Gelaro, R., McCarty, W., Suárez, M. J., Todling, R., Molod, A., Takacs, L., et al. (2017). The modern-era retrospective analysis for research and applications, version 2 (MERRA-2). *Journal of Climate*, *30*(14), 5419–5454. https://doi.org/10.1175/JCLI-D-16-0758.1

Gerard, G., & Chanton, J. (1993). Quantification of methane oxidation in the rhizosphere of emergent aquatic macrophytes: Defining upper limits. *Biogeochemistry*, *23*(2), 79–97. https://doi.org/10.1007/BF00000444

Global Soil Data Task Group. (2000). Global gridded surfaces of selected soil characteristics (IGBP-DIS). ORNL DAAC, Oak Ridge, Tennessee, USA. https://doi.org/10.3334/ORNLDAAC/569.

Goodrich, J. P., Campbell, D. I., Roulet, N. T., Clearwater, M. J., & Schipper, L. A. (2015). Overriding control of methane flux temporal variability by water table dynamics in a Southern Hemisphere, raised bog. *Journal of Geophysical Research: Biogeosciences*, *120*(5), 819–831. https://doi.org/10.1002/2014JG002844

Granberg, G., Ottosson-Löfvenius, M., Grip, H., Sundh, I., & Nilsson, M. (2001). Effect of climatic variability from 1980 to 1997 on simulated methane emission from a boreal mixed mire in northern Sweden. *Global Biogeochemical Cycles*, *15*(4), 977–991. https://doi.org/10.1029/2000GB001356

Grant, R. F. (1998). Simulation of methanogenesis in the mathematical model ecosys. *Soil Biology and Biochemistry*, *30*(7), 883–896. https://doi.org/10.1016/S0038-0717(97)00218-6

Grant, R. F. (1999). Simulation of methanotrophy in the mathematical model ecosys. *Soil Biology and Biochemistry*, *31*(2), 287–297. https://doi.org/10.1016/S0038-0717(98)00119-9

Grant, R. F., & Roulet, N. T. (2002). Methane efflux from boreal wetlands: Theory and testing of the ecosystem model ecosys with chamber and tower flux measurements. *Global Biogeochemical Cycles*, *16*(4), 1054. https://doi.org/10.1029/2001GB001702

Green, S. M., & Baird, A. J. (2012). A mesocosm study of the role of the sedge Eriophorum angustifolium in the efflux of methane–including that due to episodic ebullition–from peatlands. *Plant and Soil*, *351*, 207–218. https://doi.org/10.1007/s11104-011-0945-1

Hanis, K. L., Tenuta, M., Amiro, B. D., & Papakyriakou, T. N. (2013). Seasonal dynamics of methane emissions from a subarctic fen in the Hudson Bay Lowlands. *Biogeosciences*, *10*(7), 4465–4479. https://doi.org/10.5194/bg-10-4465-2013

Hartmann, D. L., Klein Tank, A. M., Rusticucci, M., Alexander, L. V., Brönnimann, S., Charabi, Y., et al. (2013). Observations: Atmosphere and Surface. In T. F. Stocker, D. Qin, G.-K. Plattner, M. Tignor, S. K. Allen, J. Boschung, A. Nauels, Y. Xia, V. Bex, & P. M. Midgley (Eds.), *Climate change 2013: The physical science basis. Contribution of Working Group I to the Fifth Assessment Report of the Intergovernmental Panel on Climate Change* (p. 159–254). Cambridge, United Kingdom and New York, NY, USA: Cambridge University Press.

Hattroi, S. (2008). Syntrophic acetate-oxidizing microbes in methanogenic environments. *Microbes and Environments*, *23*(2), 118–127. https://doi.org/10.1264/jsme2.23.118

Hirano, T., Kusin, K., Limin, S., & Osaki, M. (2014). Carbon dioxide emissions through oxidative peat decomposition on a burnt tropical peatland. *Global Biogeochemical Cycles*, *20*, 555–565. https://doi.org/10.1111/gcb.12296

Hommeltenberg, J., Mauder, M., Drösler, M., Heidbach, K., Werle, P., & Schmid, H. P. (2014). Ecosystem scale methane fluxes in a natural temperate bog-pine forest in southern Germany. *Agricultural and Forest Meteorology*, *198–199*, 273–284. https://doi.org/10.1016/j.agrformet.2014.08.017

Ito, A., & Inatomi, M. (2012). Use of a process-based model for assessing the methane budgets of global terrestrial ecosystems and evaluation of uncertainty. *Biogeosciences*, *9*(2), 759–773. https://doi.org/10.5194/bg-9-759-2012

Jackowicz-Korczyński, M., Christensen, T. R., Bäckstrand, K., Crill, P., Friborg, T., Mastepanov, M., & Ström, L. (2010). Annual cycle of methane emission from a subarctic peatland. *Journal of Geophysical Research*, *115*, G02009. https://doi.org/10.1029/2008JG000913

Joabsson, A., & Christensen, T. R. (2001). Methane emissions from wetlands and their relationship with vascular plants: An Arctic example. *Global Change Biology*, *7*, 919–932. https://doi.org/10.1046/j.1354-1013.2001.00044.x

Kaiser, S., Göckede, M., Castro-Morales, K., Knoblauch, C., Ekici, A., Kleinen, T., et al. (2017). Process-based modelling of the methane balance in periglacial landscapes (JSBACH-methane). *Geoscientific Model Development*, *10*(1), 333–358. https://doi.org/10.5194/gmd-10-333-2017

Kettunen, A. (2003). Connecting methane fluxes to vegetation cover and water table fluctuations at microsite level: A modeling study. *Global Biogeochemical Cycles*, *17*(2), 1051. https://doi.org/10.1029/2002GB001958

King, J. Y., Reeburgh, W. S., & Regli, S. K. (1998). Methane emission and transport by arctic sedges in Alaska: Results of a vegetation removal experiment. *Journal of Geophysical Research*, *103*(D22), 29,083–29,092. https://doi.org/10.1029/98JD00052

Kotsyurbenko, O. R., Glagolev, M. V., Nozhevnikova, A. N., & Conrad, R. (2001). Competition between homoacetogenic bacteria and methanogenic archaea for hydrogen at low temperature. *FEMS Microbiology Ecology*, *38*, 153–159. https://doi.org/10.1016/S0168-6496(01)00179-9

Krüger, M., Frenzel, P., & Conrad, R. (2001). Microbial processes influencing methane emission from rice fields. *Global Change Biology*, *7*(1), 49–63. https://doi.org/10.1046/j.1365-2486.2001.00395.x

Kucharik, C. J., Foley, J. A., Delire, C., Fisher, V. A., Coe, M. T., Lenters, J. D., et al. (2000). Testing the performance of a dynamic global ecosystem model: Water balance, carbon balance, and vegetation structure. *Global Biogeochemical Cycles*, *14*(3), 795–825. https://doi.org/10.1029/1999GB001138

Lai, D. Y., Moore, T. R., & Roulet, N. T. (2014). Spatial and temporal variations of methane flux measured by autochambers in a temperate ombrotrophic peatland. *Journal of Geophysical Research: Biogeosciences*, *119*, 864–880. https://doi.org/10.1002/2013JG002410

Liu, D., Chen, Y., Cai, W., Dong, W., Xiao, J., Chen, J., et al. (2014). The contribution of China's grain for green program to carbon sequestration. *Landscape Ecology*, *29*(10), 1675–1688. https://doi.org/10.1007/s10980-014-0081-4

Liu, F., & Conrad, R. (2011). Chemolithotrophic acetogenic H_2/CO_2 utilization in Italian rice field soil. *ISME Journal*, *5*(9), 1526–1539. https://doi.org/10.1038/ismej.2011.17

Liu, X., Guo, Y., Hu, H., Sun, C., Zhao, X., & Wei, C. (2015). Dynamics and controls of CO_2 and CH_4 emissions in the wetland of a montane permafrost region, northeast China. *Atmospheric Environment*, *122*, 454–462. https://doi.org/10.1016/j.atmosenv.2015.10.007

Long, K. D., Flanagan, L. B., & Cai, T. (2010). Diurnal and seasonal variation in methane emissions in a northern Canadian peatland measured by eddy covariance. *Global Change Biology*, *16*(9), 2420–2435. https://doi.org/10.1111/j.1365-2486.2009.02083.x

Ma, S., Jiang, J., Huang, Y., Shi, Z., Wilson, R. M., Ricciuto, D., et al. (2017). Data-constrained projections of methane fluxes in a northern Minnesota peatland in response to elevated CO_2 and warming. *Journal of Geophysical Research: Biogeosciences*, *122*, 2841–2861. https://doi.org/10.1002/2017JG003932

Marelli, S., Lamas, C., Konakli, K., Mylonas, C., Wiederkehr, P., & Sudret, B. (2019). UQLab user manual–Sensitivity analysis, report # UQLab-V1.3-106, Chair of Risk, Safety and Uncertainty Quantification, ETH Zurich, Switzerland.

Marushchak, M. E., Friborg, T., Biasi, C., Herbst, M., Johansson, T., Kiepe, I., et al. (2016). Methane dynamics in the subarctic tundra: Combining stable isotope analyses, plot- and ecosystem-scale flux measurements. *Biogeosciences*, *13*(2), 597–608. https://doi.org/10.5194/bg-13-597-2016

Mastepanov, M., Sigsgaard, C., Tagesson, T., Ström, L., Tamstorf, M. P., Lund, M., & Christensen, T. R. (2013). Revisiting factors controlling methane emissions from high-Arctic tundra. *Biogeosciences*, *10*(7), 5139–5158. https://doi.org/10.5194/bg-10-5139-2013

Megonigal, J. P., Hines, M. E., & Visscher, P. T. (2004). Anaerobic metabolism: Linkages to trace gases and aerobic processes. In W. H. Schlesinger (Ed.), *Biogeochemistry*, (pp. 317–424). UK, Elsevier-Pergamon: Oxford.

Melling, L., Hatano, R., & Goh, K. J. (2005). Soil CO_2 flux from three ecosystems in tropical peatland of Sarawak, Malaysia. *Tellus B*, *57*(1), 1–11. https://doi.org/10.1111/j.1600-0889.2005.00129.x

Melton, J. R., Wania, R., Hodson, E. L., Poulter, B., Ringeval, B., Spahni, R., et al. (2013). Present state of global wetland extent and wetland methane modelling: Conclusions from a model inter-comparison project (WETCHIMP). *Biogeosciences*, *10*(2), 753–788. https://doi.org/10.5194/bg-10-753-2013

Meng, L., Hess, P. G. M., Mahowald, N. M., Yavitt, J. B., Riley, W. J., Subin, Z. M., et al. (2012). Sensitivity of wetland methane emissions to model assumptions: Application and model testing against site observations. *Biogeosciences*, *9*(7), 2793–2819. https://doi.org/10.5194/bg-9-2793-2012

Mer, J. L., & Roger, P. (2001). Production, oxidation, emission and consumption of methane by soils: A review. *European Journal of Soil Biology*, *37*(1), 25–50. https://doi.org/10.1016/S1164-5563(01)01067-6

Mikhaylov, O. A., Miglovets, M. N., & Zagirova, S. V. (2015). Vertical methane fluxes in mesooligotrophic boreal peatland in European northeast Russia. *Contemporary Problems of Ecology*, *8*(3), 368–375. https://doi.org/10.1134/S1995425515030099

Moore, T. R., De Young, A., Bubier, J. L., Humphreys, E. R., Lafleur, P. M., & Roulet, N. T. (2011). A multi-year record of methane flux at the Mer Bleue bog, Southern Canada. *Ecosystems*, *14*, 646–657. https://doi.org/10.1007/s10021-011-9435-9

Morel, X., Decharme, B., Delire, C., Krinner, G., Lund, M., Hansen, B. U., & Mastepanov, M. (2019). A new process-based soil methane scheme for land surface modeling: Evaluation over Arctic field sites with the ISBA land surface model. *Journal of Advances in Modeling Earth Systems*, *11*, 293–326. https://doi.org/10.1029/2018MS001329

Münchberger, W., Knorr, K. -H., Blodau, C., Pancotto, V. A., & Kleinebecker, T. (2019). Zero to moderate methane emissions in a densely rooted, pristine Patagonian bog–Biogeochemical controls as revealed from isotopic evidence. *Biogeosciences*, *16*(2), 541–559. https://doi.org/10.5194/bg-16-541-2019

Myhre, G., Shindell, D., Bréon, F.-M., Collins, W., Fuglestvedt, J., Huang, J., et al. (2013). Anthropogenic and natural radiative forcing. In T. F. Stocker, D. Qin, G.-K. Plattner, M. Tignor, S. K. Allen, J. Boschung, A. Nauels, Y. Xia, V. Bex, & P. M. Midgley (Eds.), *Climate change 2013: The physical science basis. Contribution of Working Group I to the Fifth Assessment Report of the Intergovernmental Panel on Climate Change*, (pp. 659–740). Cambridge, UK and New York, NY, USA: Cambridge University Press.

Nadeau, D. F., Rousseau, A. N., Coursolle, C., Margolis, H. A., & Parlange, M. B. (2013). Summer methane fluxes from a boreal bog in northern Quebec, Canada, using eddy covariance measurements. *Atmospheric Environment*, *81*, 464–474. https://doi.org/10.1016/j.atmosenv.2013.09.044

Noyce, G. L., Varner, R. K., Bubier, J. L., & Frolking, S. (2014). Effect of Carex rostrata on seasonal and interannual variability in peatland methane emissions. *Journal of Geophysical Research: Biogeosciences*, *119*, 24–34. https://doi.org/10.1002/2013JG002474

Olson, D. M., Griffis, T. J., Noormets, A., Kolka, R., & Chen, J. (2013). Interannual, seasonal, and retrospective analysis of the methane and carbon dioxide budgets of a temperate peatland. *Journal of Geophysical Research: Biogeosciences*, *118*, 226–238. https://doi.org/10.1002/jgrg.20031

Petrescu, A. M. R., van Huissteden, J., Jackowicz-Korczynski, M., Yurova, A., Christensen, T. R., Crill, P. M., et al. (2008). Modelling CH_4 emissions from Arctic wetlands: Effects of hydrological parameterization. *Biogeosciences*, *5*(1), 111–121. https://doi.org/10.5194/bg-5-111-2008

Press, W. H., Teukolsky, S. A., Vetterling, W. T., & Flannery, B. P. (1996). *Numerical recipes in Fortran 90: The art of parallel scientific computing*, (2nd ed.). New York: Cambridge University Press.

Raivonen, M., Smolander, S., Backman, L., Susiluoto, J., Aalto, T., Markkanen, T., et al. (2017). HIMMELI v1.0: HelsinkI Model of MEthane buiLdup and emIssion for peatlands. *Geoscientific Model Development*, *10*(12), 4665–4691. https://doi.org/10.5194/gmd-10-4665-2017

Ricciuto, D., Sargsyan, K., & Thornton, P. (2018). The impact of parametric uncertainties on biogeochemistry in the E3SM land model. *Journal of Advances in Modeling Earth Systems*, *10*, 297–319. https://doi.org/10.1002/2017MS000962

Riley, W. J., Subin, Z. M., Lawrence, D. M., Swenson, S. C., Torn, M. S., Meng, L., et al. (2011). Barriers to predicting changes in global terrestrial methane fluxes: Analyses using CLM4Me, a methane biogeochemistry model integrated in CESM. *Biogeosciences*, *8*, 1925–1953. https://doi.org/10.5194/bg-8-1925-2011

Ringeval, B., de Noblet-Ducoudré, N., Ciais, P., Bousquet, P., Prigent, C., Para, F., & Rossow, W. B. (2010). An attempt to quantify the impact of changes in wetland extent on methane emissions on the seasonal and interannual time scales. *Global Biogeochemical Cycles*, *24*, GB2003. https://doi.org/10.1029/2008GB003354

Ringeval, B., Friedlingstein, P., Koven, C., Ciais, P., de NobletDucoudré, N., Decharme, B., & Cadule, P. (2011). Climate-CH_4 feedback from wetlands and its interaction with the climate-CO_2 feedback. *Biogeosciences*, *8*(8), 2137–2157. https://doi.org/10.5194/bg-8-2137-2011

Rinne, J., Tuittila, E.-S., Peltola, O., Li, X., Raivonen, M., Alekseychik, P., et al. (2018). Temporal variation of ecosystem scale methane emission from a boreal fen in relation to temperature, water table position, and carbon dioxide fluxes. *Global Biogeochemical Cycle*, *32*, 1087–1106. https://doi.org/10.1029/2017GB005747

Sander, R. (2015). Compilation of Henry's law constants (version 4.0) for water as solvent. *Atmospheric Chemistry and Physics*, *15*(8), 4399–4981. https://doi.org/10.5194/acp-15-4399-2015

Sangok, F. E., Maie, N., Melling, L., & Watanabe, A. (2017). Evaluation on the decomposability of tropical forest peat soils after conversion to an oil palm plantation. *Science of the Total Environment*, *587*, 381–388. https://doi.org/10.1016/j.scitotenv.2017.02.165

Saunois, M., Bousquet, P., Poulter, B., Peregon, A., Ciais, P., Canadell, J. G., et al. (2016). The global methane budget 2000–2012. *Earth System Science Data*, *8*(2), 697–751. https://doi.org/10.5194/essd-8-697-2016

Schulz, S., & Conrad, R. (1996). Influence of temperature on pathways to methane production in the permanently cold profundal sediment of Lake Constance. *FEMS Microbiology Ecology*, *20*(1), 1–14. https://doi.org/10.1016/0168-6496(96)00009-8

Shannon, R. D., & White, J. R. (1994). A three-year study of controls on methane emissions from two Michigan peatlands. *Biogeochemistry*, *27*(1), 35–60. https://doi.org/10.1007/BF00002570

Shi, Y., Gong, W., Duan, Q., Charles, J., Xiao, C., & Wang, H. (2019). How parameter specification of an earth system model of intermediate complexity influences its climate simulations. *Progress in Earth and Planetary Science.*, *6*(1), 1–18. https://doi.org/10.1186/s40645-019-0294-x

Smemo, K. A., & Yavitt, J. B. (2011). Anaerobic oxidation of methane: An underappreciated aspect of methane cycling in peatland ecosystems? *Biogeosciences*, *8*(3), 779–793. https://doi.org/10.5194/bg-8-779-2011

Sobol, I. M. (1993). Sensitivity estimates for nonlinear mathematical models. *Mathematical Modeling and Computational Experiment*, *1*, 407–414.

Song, W., Wang, H., Wang, G., Chen, L., Jin, Z., Zhuang, Q., & He, J.-S. (2015). Methane emissions from an alpine wetland on the Tibetan Plateau: Neglected but vital contribution of the nongrowing season. *Journal of Geophysical Research: Biogeosciences*, *120*, 1475–1490. https://doi.org/10.1002/2015JG003043

Stephen, K. D., Arah, J. R. M., Daulat, W., & Clymo, R. S. (1998). Root-mediated gas transport in peat determined by argon diffusion. *Soil Biology and Biochemistry*, *30*(4), 501–508. https://doi.org/10.1016/S0038-0717(97)00142-9

Strachanm, I. B., Nugent, K. A., Crombie, S., & Bonneville, M. (2015). Carbon dioxide and methane exchange at a cool-temperate freshwater marsh. *Environmental Research Letters*, *10*(6). https://doi.org/10.1088/1748-9326/10/6/065006

Sturtevant, C., Ruddell, B. L., Knox, S. H., Verfaillie, J., Matthes, J. H., Oikawa, P. Y., & Baldocchi, D. (2016). Identifying scale-emergent, nonlinear, asynchronous processes of wetland methane exchange. *Journal of Geophysical Research: Biogeosciences*, *121*, 188–204. https://doi.org/10.1002/2015JG003054

Sudret, B. (2008). Global sensitivity analysis using polynomial chaos expansions. *Reliability Engineering & System Safety*, *93*(7), 964–979. https://doi.org/10.1016/j.ress.2007.04.002

Sun, L., Song, C., Lafleur, P. M., Miao, Y., Wang, X., Gong, C., et al. (2018). Wetland-atmosphere methane exchange in northeast China: A comparison of permafrost peatland and freshwater wetlands. *Agricultural and Forest Meteorology*, *249*, 239–249. https://doi.org/10.1016/j.agrformet.2017.11.009

Sun, L., Song, C., Miao, Y., Qiao, T., & Gong, C. (2013). Temporal and spatial variability of methane emissions in a northern temperate marsh. *Atmospheric Environment*, *81*, 356–363. https://doi.org/10.1016/j.atmosenv.2013.09.033

Tang, A. C. I., Stoy, P. C., Hirata, R., Musin, K. K., Aeries, E. B., Wenceslaus, J., & Melling, L. (2018). Eddy covariance measurements of methane flux at a tropical peat forest in Sarawak, Malaysian Borneo. *Geophysical Research Letters*, *45*, 4390–4399. https://doi.org/10.1029/2017GL076457

Tang, J., Zhuang, Q., Shannon, R. D., & White, J. R. (2010). Quantifying wetland methane emissions with process-based models of different complexities. *Biogeosciences*, *7*(11), 3817–3837. https://doi.org/10.5194/bg-7-3817-2010

Tian, H., Xu, X., Liu, M., Ren, W., Zhang, C., Chen, G., & Lu, C. (2010). Spatial and temporal patterns of CH_4 and N_2O fluxes in terrestrial ecosystems of North America during 1979–2008: Application of a global biogeochemistry model. *Biogeosciences*, *7*(9), 2673–2694. https://doi.org/10.5194/bg-7-2673-2010

Tokida, T., Miyazaki, T., Mizoguchi, M., Nagata, O., Takakai, F., Kagemoto, A., & Hatano, R. (2007). Falling atmospheric pressure as a trigger for methane ebullition from peatland. *Global Biogeochemical Cycles*, *21*, GB2003. https://doi.org/10.1029/2006GB002790

Van den Berg, M., Ingwersen, J., Lamers, M., & Streck, T. (2016). The role of phragmites in the CH_4 and CO_2 fluxes in a minerotrophic peatland in southwest Germany. *Biogeosciences*, *13*(21), 6107–6119. https://doi.org/10.5194/bg-13-6107-2016

Van Huissteden, J., Van den Bos, R., & Marticorena Alvarez, I. (2006). Modeling the effect of water-table management on CO_2 and CH_4 fluxes from peat soils. *Netherlands Journal of Geosciences*, *85*(1), 3–18. https://doi.org/10.1017/S0016774600021399

Waddington, J. M., Roulet, N. T., & Swanson, R. V. (1996). Water table control of CH_4 emission enhancement by vascular plants in boreal peatlands. *Journal of Geophysical Research*, *101*(D17), 22,775–22,785. https://doi.org/10.1029/96JD02014

Walter, B. P., & Heimann, M. (2000). A process-based climate-sensitive model to derive methane emissions from natural wetlands: Application to five wetland sites, sensitivity to model parameters, and climate. *Global Biogeochemical Cycles*, *14*(3), 745–765. https://doi.org/10.1029/1999GB001204

Wang, C., Duan, Q., Tong, C. H., Di, Z., & Gong, W. (2016). A GUI platform for uncertainty quantification of complex dynamical models. *Environmental Modelling & Software*, *76*(C), 1–12. https://doi.org/10.1016/j.envsoft.2015.11.004

Wang, M., Wu, J., Lafleur, P. M., Luan, J., Chen, H., & Zhu, X. (2018). Temporal shifts in controls over methane emissions from a boreal bog. *Agricultural and Forest Meteorology*, *262*, 120–134. https://doi.org/10.1016/j.agrformet.2018.07.002

Wania, R., Ross, I., & Prentice, I. C. (2010). Implementation and evaluation of a new methane model within a dynamic global vegetation model: LPJ-WHyMe v1.3.1. *Geoscientific Model Development*, *3*(2), 565–584. https://doi.org/10.5194/gmd-3-565-2010

Whalen, S. C. (2005). Biogeochemistry of methane exchange between natural wetlands and the atmosphere. *Environmental Engineering Science*, *22*(1), 73–94. https://doi.org/10.1089/ees.2005.22.73

Whiting, G. J., & Chanton, J. P. (1992). Plant-dependent methane emission in a subarctic Canadian fen. *Global Biogeochemical Cycles*, *6*(3), 225–231. https://doi.org/10.1029/92GB00710

Whiting, G. J., & Chanton, J. P. (1996). Control of the diurnal pattern of methane emission from emergent aquatic macrophytes by gas transport mechanisms. *Aquatic Botany*, *54*, 237–253. https://doi.org/10.1016/0304-3770(96)01048-0

Wille, C., Kutzbach, L., Sachs, T., Wagner, D., & Pfeiffer, E.-M. (2008). Methane emission from Siberian arctic polygonal tundra: Eddy covariance measurements and modeling. *Global Change Biology*, *14*(6), 1395–1408. https://doi.org/10.1111/j.1365-2486.2008.01586.x

Wong, G. X., Hirata, R., Hirano, T., Kiew, F., Aeries, E. B., Musin, K. K., et al. (2018). Micrometeorological measurement of methane flux above a tropical peat swamp forest. *Agricultural and Forest Meteorology*, *256–257*, 353–361. https://doi.org/10.1016/j.agrformet.2018.03.025

Xu, X., Elias, D. A., Graham, D. E., Phelps, T. J., Carroll, S. L., Wullschleger, S. D., & Thornton, P. E. (2015). A microbial functional group-based module for simulating methane production and consumption: Application to an incubated permafrost soil. *Journal of Geophysical Research: Biogeosciences*, *120*, 1315–1333. https://doi.org/10.1002/2015JG002935

Xu, X., Yuan, F., Hanson, P. J., Wullschleger, S. D., Thornton, P. E., Riley, W. J., et al. (2016). Reviews and syntheses: Four decades of modeling methane cycling in terrestrial ecosystems. *Biogeosciences*, *13*(12), 3735–3755. https://doi.org/10.5194/bg-13-3735-2016

Yuan, W., Liu, D., Dong, W., Liu, S., Zhou, G., Yu, G., et al. (2014). Multiyear precipitation reduction strongly decreases carbon uptake over northern China. *Journal of Geophysical Research: Biogeosciences*, *119*, 881–896. https://doi.org/10.1002/2014JG002608

Zhang, Y., Li, C., Trettin, C. C., Li, H., & Sun, G. (2002). An integrated model of soil, hydrology, and vegetation for carbon dynamics in wetland ecosystems. *Global Biogeochemical Cycles*, *16*(4), 1061. https://doi.org/10.1029/2001GB001838

Zhu, Q., Liu, J., Peng, C., Chen, H., Fang, X., Jiang, H., et al. (2014). Modelling methane emissions from natural wetlands by development and application of the TRIPLEX-GHG model. *Geoscientific Model Development*, *7*(3), 981–999. https://doi.org/10.5194/gmd-7-981-2014

Zhuang, Q., Melillo, J. M., Kicklighter, D. W., Prinn, R. G., McGuire, A. D., Steudler, P. A., et al. (2004). Methane fluxes between terrestrial ecosystems and the atmosphere at northern high latitudes during the past century: A retrospective analysis with a process-based biogeochemistry model. *Global Biogeochemical Cycles*, *18*, GB3010. https://doi.org/10.1029/2004GB002239